# Simultaneous J-, H-, K- and L-band spectroscopic observations of galactic Be stars ⋆

## I. IR atlas

Y.R. Cochetti[1,2,⋆⋆], M.L. Arias[1,2,⋆⋆⋆], L.S. Cidale[1,2,⋆⋆⋆], A. Granada[3,⋆⋆⋆], and A.F. Torres[1,2,⋆⋆⋆]

[1] Instituto de Astrofísica de La Plata (CCT La Plata - CONICET, UNLP), Paseo del Bosque S/N, La Plata, B1900FWA, Buenos Aires, Argentina
e-mail: cochetti@fcaglp.unlp.edu.ar
[2] Departamento de Espectroscopía, Facultad de Ciencias Astronómicas y Geofísicas, Universidad Nacional de La Plata
[3] Centro Interdisciplinario de Telecomunicaciones, Electrónica, Computación y Ciencia Aplicada (CITECCA), Sede Andina, Universidad Nacional de Río Negro, Anasagasti 1463, San Carlos de Bariloche, Río Negro, Argentina

## ABSTRACT

*Context.* It is already accepted that Be stars are surrounded by circumstellar envelopes, which are mostly compatible with a disc geometry in Keplerian rotation. Their infrared region is characterised by a moderate flux excess and the presence of hydrogen recombination lines that allow us to obtain information on the physical and dynamical structure of different regions inside the disc. Nevertheless, many of the infrared studies available in the literature show low-resolution spectra, or are restricted to a small object sample or describe just an individual object. Some others analyse reduced spectral ranges or just one infrared band.
*Aims.* We aim to obtain a more complete characterisation of the properties of the circumstellar environment of Be stars that helps to constrain the theoretical models of the Be phenomenon.
*Methods.* Throughout the last decade, we used the spectroscopic facilities at the Gemini and Las Campanas observatories to obtain quasi-simultaneous spectra in the J, H, K, and L bands of a sample of Be stars with medium resolution.
*Results.* We present near-infrared, medium-resolution spectra of a sample of galactic Be stars with different spectral subtypes and luminosity classes. We measure different parameters of the hydrogen recombination lines from the Paschen, Brackett, Pfund, and Humphreys series, and use them to diagnose physical conditions in the circumstellar environment. We analysed the equivalent-width (EW) ratio between Br$\alpha$ and Br$\gamma$ lines and different diagrams of flux ratios. We also identify lines from He ɪ, C ɪ, N ɪ, O ɪ, Na ɪ, Mg ɪ, Mg ɪɪ, Si ɪ, Fe ɪ, and Fe ɪɪ. Analysing the EW measurements of particular He ɪ, Mg ɪɪ, Fe ɪ, Fe ɪɪ and O ɪ lines, we find that for some lines they correlate with the spectral type of the star. Particularly, the emission of the O ɪ $\lambda$ 1.3168 $\mu$m line decreases towards the later spectral types.
*Conclusions.* We present an atlas of 22 Be stars, that covers a wide infrared (IR) spectral range with quasi-simultaneous observations. From a detailed analysis, we define new complementary criteria to Mennickent's classification of Be stars according to their disc opacity. Some objects in our sample present compact thick envelopes, while in others the envelope is extended and optically thin. The correlation between the full widths at half maximum (FWHM) and the peak separation ($\Delta$V) versus $V \sin i$ for the Br10, Br$\delta$, and Hu14 lines reveals that the broadening mechanism is rotational. The Ly$\beta$ fluorescence is a key mechanism to explain the intensity of the emission of Mg ɪɪ and O ɪ lines.

**Key words.** Techniques: spectroscopic – circumstellar matter – Stars: emission-line, Be

## 1. Introduction

Be stars are rapidly rotating, non-supergiant B-type stars, whose spectra show or have shown the H$\alpha$ line in emission (Jaschek et al. 1981; Collins 1987). It is already accepted that these objects present circumstellar envelopes, mostly compatible with a disc geometry in Keplerian rotation (Rivinius et al. 2013). The infrared (IR) part of their spectra is characterised by a moderate flux excess and the presence of numerous hydrogen emission lines of the Paschen, Brackett, Pfund, and Humphreys series. These lines are formed in a region more internal than that of the optical H lines, and, for most of them, the photospheric absorption contribution is negligible (Steele & Clark 2001; Lenorzer et al. 2002b). Thus, they allow us to obtain information on the physical and dynamical structure of different regions within the

disc (Hony et al. 2000; Lenorzer et al. 2002a; Mennickent et al. 2009; Granada et al. 2010; Sabogal et al. 2017).

While different studies devoted to the near-IR spectra of Be stars show low-resolution data, many of them are restricted to a small sample, and some others analyse reduced spectral ranges. For instance, there are only a few studies done in the J band, and they focus mainly on a particular object or a specific spectral line or element (Mathew et al. 2012a,b; Štefl et al. 2009). Also, individual spectral ranges have already been studied for large samples of Be stars. Steele & Clark (2001) presented H-band spectroscopy of Be stars with a spectral resolution of R ≃ 3 000. They reported Brackett and Fe II lines in emission and, from the analysis of the strength ratio of the higher Brackett lines to Brγ, were able to distinguish early- from late-type Be stars. Later, Chojnowski et al. (2015) published high-resolution H-band spectroscopy for a great number of Be stars observed with APOGEE. They found that the Br11 emission line is formed preferentially in a circumstellar disc at an average distance of ~ 2.2 $R_\star$, while the higher Brackett lines seem to originate in an innermost region. Several emission lines have been identified for the first time, such as C I $\lambda\,1.6895\,\mu m$, which is also formed in the inner region of the discs. In a later work, Chojnowski et al. (2017) analysed the variation of the emission strength, peak intensity ratio, and peak separation. Their analysis revealed a variety of temporal variability, including the disappearance and appearance of the line emission on different timescales. In the K band, Hanson et al. (1996), Clark & Steele (2000) and Granada et al. (2010) reported Brγ, Brδ, and Pfund lines in emission together with lines of He I in emission or absorption, and Mg II, Fe II and Na I lines in emission. Clark & Steele (2000) related the infrared characteristics to the underlying properties of the stars: objects that present He I features in emission or absorption are B3 or earlier; if the star presents Mg II in emission but no He I, it is between B2 and B4; objects with Brγ emission but no evidence of He I or Mg II are B5 or later. Lenorzer et al. (2002b) provided an extensive atlas of early type stars, including a number of Be stars, covering the K and L bands, while Lenorzer et al. (2002a) analysed the H recombination lines of those stars and constructed a diagram of flux ratios of some selected recombination lines: Hu14/Brα and Hu14/Pfγ. In this diagram, the location of the objects gives information about the density of the emitting gas. After that, Mennickent et al. (2009) presented a classification scheme for Be stars based on the intensity of the L-band hydrogen-emission lines. The objects in each group fall in different regions of Lenorzer's diagram; thus, this classification scheme is probably connected to the density of the disc. Granada et al. (2010) analysed a sample of eight Be stars and classified them with Mennickent's criterion. They found that for group I objects, the equivalent widths (EW) of Brα and Brγ lines are similar, while for stars in group II the EW(Brγ) is much larger (more than five times) than the EW(Brα). Besides this, Mennickent et al. (2009) and Granada et al. (2010) reported emission lines not only in Brα, Pfγ, and the Humphreys series but also in He I $\lambda\,4.038\,\mu m$ and He I $\lambda\,4.041\,\mu m$. Sabogal et al. (2017) showed a sample of L-band Be-star spectra and correlated the infrared features with the optical Hα line behaviour.

Despite the broad studies performed in the near-IR (NIR) bands, an analysis of Be stars observed (quasi) simultaneously in the whole range (0.8 − 4.5 $\mu m$) is still lacking. In order to obtain a more complete picture of the properties of their circumstellar environment, we collected a great number of NIR spectra of Be stars that cover a wider spectral range than those reported in previous works. These spectra together with the results we obtained from them, will be presented in a series of future papers. In this first work we present a medium resolution (R∼1 800 and R∼6 000) spectral atlas of a sample of 22 galactic Be stars, observed quasi-simultaneously in the J, H, K, and L bands. The paper is organised as follows. In Sect. 2 we present the observations. In Sect. 3 we present and describe the spectra and highlight their main features. The discussion is presented in Sect. 4, and our conclusions are in Sect. 5. The circumstellar parameters derived from the lines described here will be presented in the second paper of this series.

## 2. Observations

Medium-resolution NIR spectra were obtained for 22 galactic Be stars with spectral types in the O7.5-A0 range and different luminosity classes. The objects were selected either due to their reported variability (Hubert & Floquet 1998; Mennickent et al. 2009; Granada et al. 2010) or the fact that they have envelope sizes determined by interferometric techniques (Cochetti et al. 2019). This allows us to analyse the evolution of the circumstellar envelopes, with the aim of performing a more complete analysis by adding IR spectroscopic observations.

The observed Be stars are listed in Table 1, which provides information about the HD name, alternative name, spectral type (ST), luminosity class (LC), projected rotational velocity ($V \sin i$), effective temperature ($T_{eff}$), and surface gravity (log $g$).

Observations were performed between 2010 and 2017 using Gemini Near-Infrared Spectrograph (GNIRS; Elias et al. 2006a,b), mounted on the Gemini North telescope, under the following programmes: GN-2010B-Q-2, GN-2012B-Q-56, GN-2016B-Q-83, GN-2017A-Q-84, GN-2017A-Q-89, GN-2017B-Q-81, and GN-2017B-Q-86. In Table 2, we describe the instrumental configurations in longslit or cross-dispersed mode that were used. These configurations provide a resolving power of R ∼ 1800.

In addition, in 2017, we performed observations with the Folded-port InfraRed Echellette (FIRE) spectrometer at Las Campanas Observatory (LCO), Chile. FIRE spectra were obtained with the high-resolution echellete mode covering the 0.8-2.5 $\mu m$ range with a resolving power of R ∼ 6000.

For the data obtained in both telescopes, the reduction procedure is similar. Several ABBA sequences were taken for each target. Flats and comparison arc lamps were taken with each source and telluric-standard star pair. We used the IRAF[1] software package tasks to extract and calibrate the GNIRS spectra and the IDL pipeline provided by Las Campanas Observatory to process FIRE observations. Data reduction steps consisted of subtracting of the AB pairs, flat-fielding, telluric-correction and wavelength and flux calibrations.

To perform the telluric and instrumental corrections, we used late-B- or early-A-type telluric standard stars, observed near the object in both time and sky position (air mass). The telluric spectrum was used to divide each programme's object spectrum to obtain a telluric-corrected one. Correction for telluric lines is often a difficult task, and, in many cases, we were not able to cancel them out completely. Thus, some residuals of the telluric lines remained in a few spectra, especially at the end of each band and particularly around 2 $\mu m$ (K band). However, this effect does not significantly affect the profile of the emission lines, except for the weakest ones.

---

[1] IRAF is distributed by the National Optical Astronomy Observatory, which is operated by the Association of Universities for Research in Astronomy (AURA) under cooperative agreement with the National Science Foundation.

**Table 1.** Fundamental parameters for the programme's Be stars.

| HD | Name | ST[a] | LC[a] | $V \sin i$[b] [km/s] | $T_{\rm eff}$[b] [K] | $\log g$[b] [dex] |
|---|---|---|---|---|---|---|
| HD 20336 | BK Cam | B2.5 | V | 341 ± 23 | 18684±517 | 3.865±0.072 |
| HD 23862 | 28 Tau | B8 | V | 290 ± 15 | 12106±272 | 3.937±0.052 |
| HD 25940 | 48 Per | B3 | V | 220 ± 13 | 16258±582 | 3.572±0.084 |
| HD 28497 | 228 Eri | B2 | V | 342 ± 24 | 26724±427 | 4.200±0.046 |
| HD 29441 | V1150 Tau | B2.5 | V | 274 ± 42[c] | 18000[g] | 3.8[g] |
| HD 32991 | 105 Tau | B2 | V | 175 ± 18[d] | 20900[h] | 3.77[h] |
| HD 35439 | $\psi_{01}$ Ori | B1 | V | 266 ± 13 | 22134±665 | 3.920±0.087 |
| HD 36576 | 120 Tau | B2 | IV-V | 266 ± 13 | 22618±508 | 3.804±0.062 |
| HD 37490 | $\omega$ Ori | B3 | V | 155 ± 5 [e] | 14492[h] | 3.86[h] |
| HD 41335 | V696 Mon | B3-5 | V | 376 ± 26 | 20902±610 | 3.886±0.081 |
| HD 68980 | MX Pup | B1.5 | IV | 152 ± 8 | 25126±642 | 3.951±0.077 |
| HD 142983 | 48 Lib | B3 [f] | V [f] | 407 ± 22 | 17642±554 | 3.845±0.080 |
| HD 155806 | V1075 Sco | O7.5 | V | 105 ± 16[c] | 34000[i] | 4.0[i] |
| HD 164284 | 66 Oph | B2 | V | 287 ± 21 | 21609±523 | 3.943±0.068 |
| HD 171623 | HR 6977 | A0 | V | 253 ± 38[c] | 9853±291 [j] | 3.91±0.23 [j] |
| HD 178175 | V4024 Sgr | B2 | V | 111 ± 7 | 18939±286 | 3.489±0.035 |
| HD 183656 | V923 Aql | B7 | III | 284 ± 16 | 12626±524 | 3.295±0.081 |
| HD 187811 | 12 Vul | B2.5 | V | 258 ± 13 | 18086±583 | 3.810±0.083 |
| HD 191610 | 28 Cyg | B2.5 | V | 318 ± 22 | 18353±516 | 3.718±0.072 |
| HD 209409 | $o$ Aqr | B7 | IV | 282 ± 20 | 12942±402 | 3.701±0.067 |
| HD 212571 | $\pi$ Aqr | B1 | III-IV | 233 ± 15 | 26061±736 | 3.915±0.088 |
| HD 217050 | EW Lac | B4 | III | 355 ± 25 | 17893±509 | 3.571±0.070 |

**References.** (a) CDS database, except other source is indicated; (b) Frémat et al. (2005), except other source is indicated; (c) Głębocki & Gnaciński (2005); (d) Abt et al. (2002); (e) Chauville et al. (2001); (f) Zorec et al. (2005). (g) using $T_{\rm eff}$ y $\log g$ from other stars with the same ST; (h) Cochetti et al. (2019); (i) Cox & Pilachowski (2000); (j) Cochetti et al. (2020).

**Table 2.** Different GNIRS configurations used on each observing run.

| Year | Mode | Camera | Disperser | Slit | Bands |
|---|---|---|---|---|---|
| 2010 | LS | short blue (0.15"/pix) | 32 l/mm | 0.3" | H-K |
| | | short red (0.15"/pix) | 32 l/mm | 0.3" | L |
| 2012 | LS | short blue (0.15"/pix) | 32 l/mm | 0.3" | H-K |
| | | long red (0.05"/pix) | 101 l/mm | 0.1" | L |
| 2016/2017 | XD | short blue (0.15"/pix) | 32 l/mm | 0.3" | J-H-K |
| | LS | long red (0.05"/pix) | 10 l/mm | 0.1" | L |

The wavelength calibration was performed using a calibration lamp, except in the case of the L-band spectra, where we used the telluric lines. Because of the small number of telluric lines available in the standard star spectrum that can be used as wavelength reference, some L-band spectra show a less precise wavelength calibration.

To flux-calibrate Gemini spectra, we used the telluric spectra subtracted by the hydrogen absorption lines as flux standards. Finally, the spectra were corrected for heliocentric velocities.

In FIRE spectra there are gaps in the regions between orders; for example, around $2.28\,\mu$m. Table 3 gives the log of the quasi-simultaneous observations, which includes, for each observed Be star, spectrograph, the observing date and observed bands. For the objects for which the time separation between the two observations is longer than ten days, we checked in the BeSS database if the star spectrum showed variations in the optical range between those dates. In all the cases, the H$\alpha$ profile remained very similar.

## 3. Results

In the following sub-sections, we present and describe the main features that characterise the NIR spectra for the programme's Be stars. Figures 1, 2, and A.1 to A.4 show the complete set of spectra, which were normalised and vertically shifted to ease inspection and comparison. The spectra are organised according to the spectral type of the star, and the positions of the identified features are labelled. The spectral regions with telluric residual lines are marked with the $\oplus$ symbol. Figures A.5 and A.6 present the line profiles of the most intense lines, Pa$\alpha$ and Br$\alpha$, which are overlapped in the complete spectra figures.

### 3.1. Hydrogen recombination lines

Our spectra cover a wide spectral range, where we have identified the following recombination hydrogen (H) lines: Pa$\alpha$ and Pa$\beta$; Br$\alpha$, and Br$\gamma$ up to the end of the series; Pf$\gamma$, Pf$\delta$, and Pf16 up to the end of the series; and Hu13 up to the end of the series. The H lines present different types of profiles. Most of the stars show H lines in emission above the continuum level, with one peak (e.g. $\Psi_{01}$ Ori) or two peaks (e.g. 12 Vul in the K band).
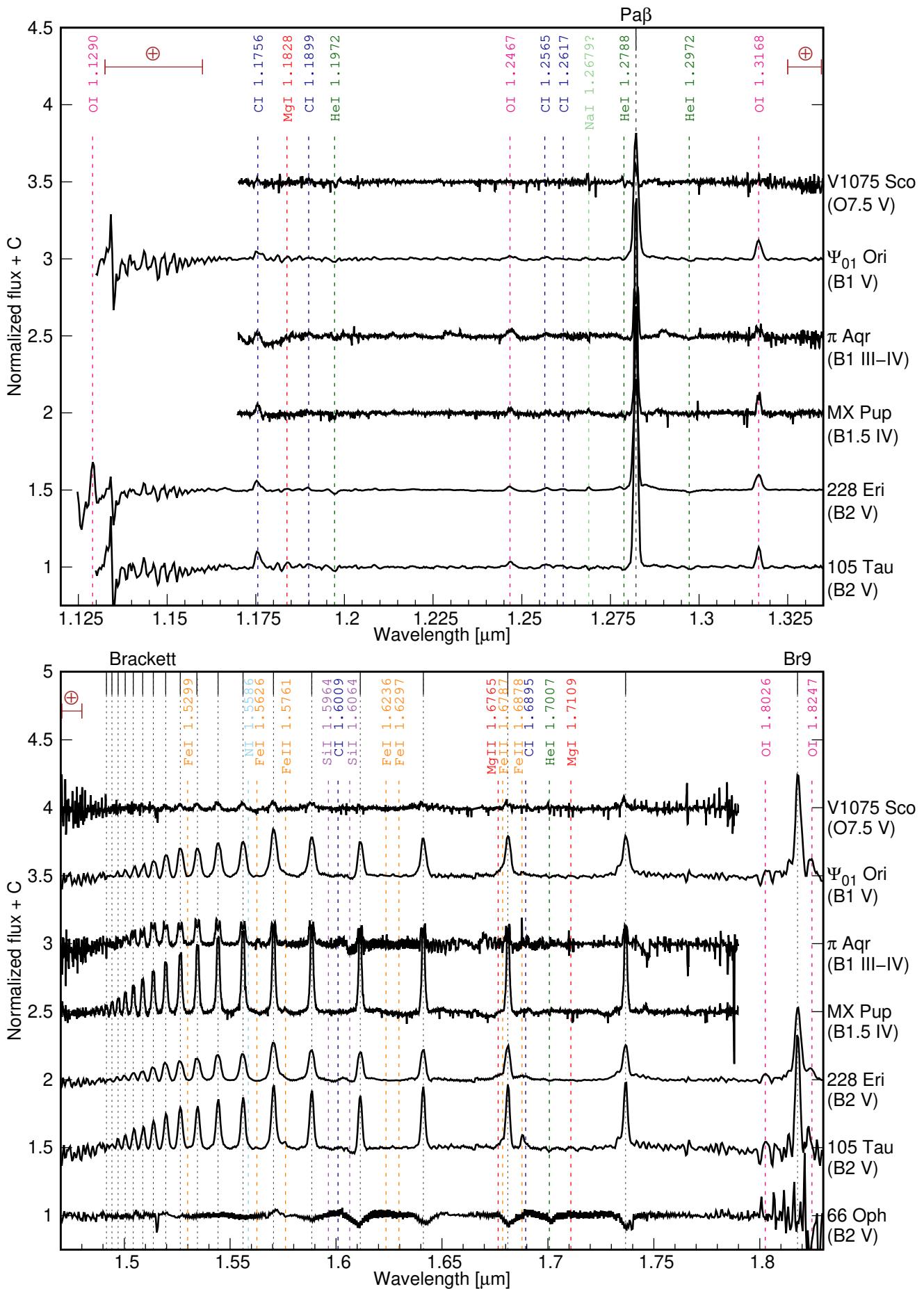
**Fig. 1.** J- (upper panel) and H-band (lower panel) spectra of Be stars. Spectra are normalised and shifted vertically to ease comparison.
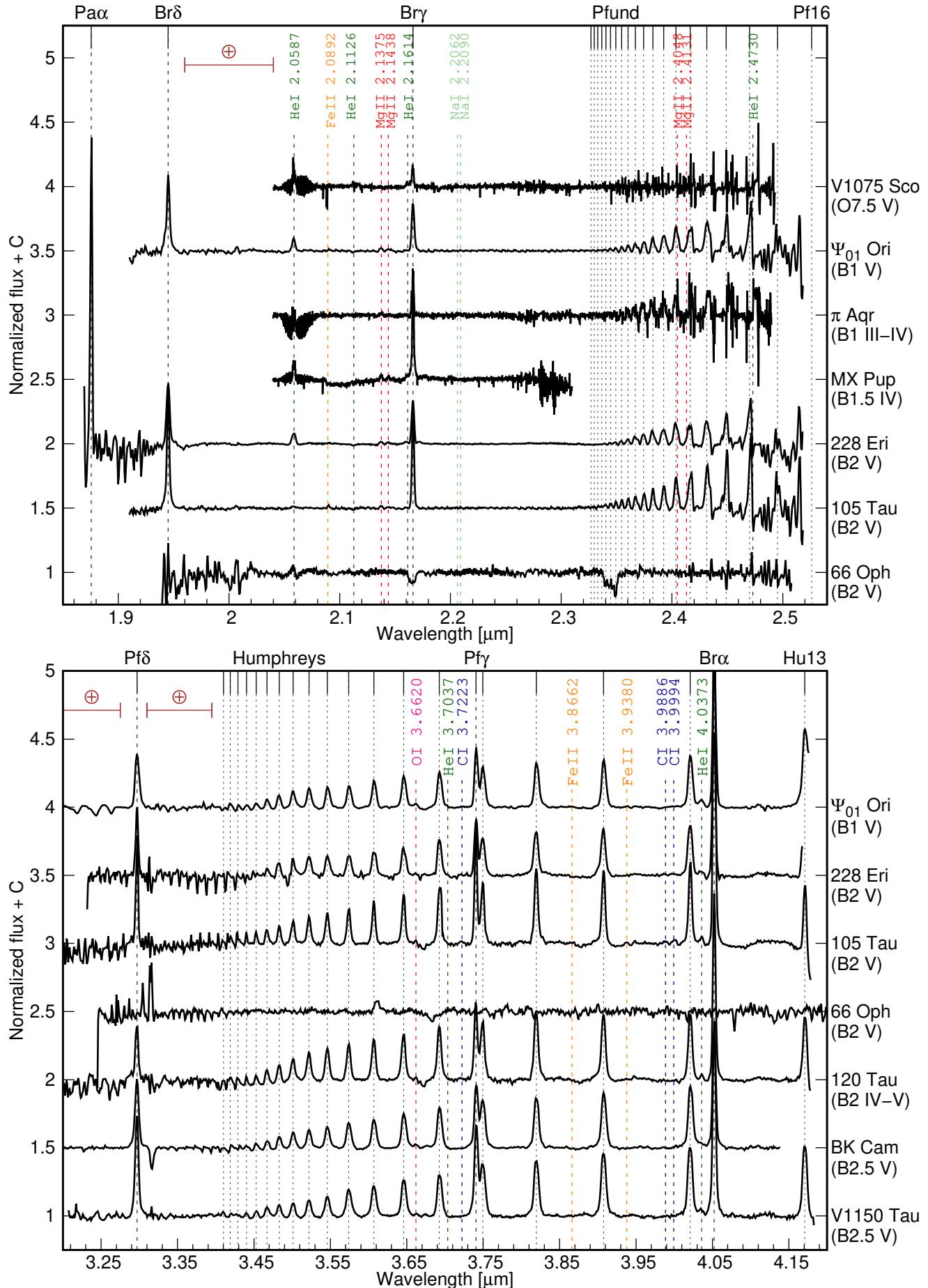
**Fig. 2.** K- (upper panel) and L-band (lower panel) spectra of Be stars. Spectra are normalised and shifted vertically to ease comparison.

**Table 3.** Log of the quasi-simultaneous observations of Be stars in the J, H, K, and L bands.

| Name | Spectrograph | Obs. date | Bands | | | |
|------|--------------|-----------|---|---|---|---|
| BK Cam | GNIRS | 2016-11-16 | J | H | K | L |
| 28 Tau | GNIRS | 2016-11-16 | | | | L |
| | | 2016-11-18 | J | H | K | |
| 48 Per | GNIRS | 2013-01-01 | | H | K | L |
| 228 Eri | GNIRS | 2017-12-10 | J | H | K | |
| | | 2017-12-14 | | | | L |
| V1150 Tau | GNIRS | 2012-12-23 | | H | K | L |
| 105 Tau | GNIRS | 2017-01-04 | J | H | K | L |
| $\psi_{01}$ Ori | GNIRS | 2017-12-14 | | | | L |
| | | 2018-01-04 | J | H | K | |
| 120 Tau | GNIRS | 2017-12-29 | J | H | K | |
| | | 2018-01-04 | | | | L |
| $\omega$ Ori | GNIRS | 2018-01-04 | J | H | K | L |
| V696 Mon | GNIRS | 2017-12-29 | J | H | K | |
| | | 2018-01-14 | | | | L |
| MX Pup | FIRE | 2017-06-03 | J | H | K | |
| 48 Lib | GNIRS | 2017-07-09 | J | H | K | |
| V1075 Sco | FIRE | 2017-06-04 | J | H | K | |
| 66 Oph | GNIRS | 2017-07-03 | J | H | K | L |
| HD 171623 | FIRE | 2017-06-04 | J | H | K | |
| V4024 Sgr | FIRE | 2017-06-04 | J | H | K | |
| V923 Aql | GNIRS | 2017-05-29 | | | | L |
| | | 2017-07-08 | J | H | K | |
| 12 Vul | GNIRS | 2010-09-15 | | H | K | L |
| 28 Cyg | GNIRS | 2017-07-09 | J | H | K | L |
| *o* Aqr | GNIRS | 2017-07-10 | J | H | K | |
| EW Lac | GNIRS | 2017-12-27 | | | | L |
| | | 2018-01-11 | J | H | K | |
| $\pi$ Aqr | FIRE | 2017-06-04 | J | H | K | |
| Observations per band | | | 19 | 22 | 22 | 15 |

There are some cases where the emission is weak and does not completely fill the photospheric absorption. In these cases the emission could be overimposed on the photospheric absorption (e.g 12 Vul in the H-band), resembling a shell-type profile (e.g. 28 Tau in the Brackett series) or barely visible as a deformation in the photospheric absorption-line profile (e.g. HD 171623 in the Pa$\beta$ and Br$\gamma$ lines). Spectra with no evidence of H emission lines are also observed (e.g. 66 Oph).

Tables 5 and B.1 to B.19 list the obtained line parameters for each object (except for 66 Oph and HD 171623, which present no evidence of H emission lines): EW, fluxes (Fl), full widths at half maximum (FWHM) and the peak separation of double-peaked line profiles ($\Delta$V). The last two values are given in units of velocity. To obtain these parameters we performed Gaussian fittings to the emission components using IRAF tasks. The uncertainties for the measurements are around 10% for EW and Fl, 75 km s$^{-1}$ for FWHM, and 25 km s$^{-1}$ for $\Delta$V. In this paper, we employ the convention that positive EW indicate emission features and negative EW indicate absorption features.

EWs and Fl for the H lines are corrected for photospheric absorption. For this purpose, we generated synthetic spectra with the SYNSPEC program (Hubeny 1988; Hubeny & Lanz 1995, 2011, 2017) using Kurucz (1979)'s atmosphere models as input. We used models with solar abundances, a microturbulence velocity of 2 km s$^{-1}$, and T$_{\text{eff}}$ and log $g$ in the ranges of 10 000 − 39 000 K and 2.5−5 dex, respectively. Steps for T$_{\text{eff}}$ and log $g$ were 1 000 K and 0.5 dex, respectively. Table 4 summarises the selected log $g$

**Table 4.** Selected log $g$ range for each T$_{\text{eff}}$ interval.

| T$_{\text{eff}}$ interval [kK] | log $g$ range (dex) |
|-------------------------------|---------------------|
| 10 - 11 | 2.0 - 5.0 |
| 12 - 19 | 2.5 - 5.0 |
| 20 - 26 | 3.0 - 5.0 |
| 27 - 31 | 3.5 - 5.0 |
| 32 - 39 | 4.0 - 5.0 |

**Table 5.** V1075 Sco - EW, Fl, and FWHM of the hydrogen lines.

| Band/line | EW | Fl | FWHM |
|-----------|------|--------|------|
| J band | | | |
| Pa$\beta$ | 4.44 | 535.85 | 197 |
| H band | | | |
| Br$_{10}$ | 3.79 | 157.54 | 313 |
| Br$_{11}$ | 3.07 | 144.84 | 438 |
| Br$_{12}$ | 2.31 | 115.05 | 529 |
| Br$_{13}$ | | em | |
| Br$_{14}$ | 1.81 | 104.26 | 502 |
| Br$_{15}$ | 1.97 | 116.7 | 478 |
| Br$_{16}$ | 1.7 | 103.57 | 509 |
| Br$_{17}$ | 1.7 | 104.69 | 540 |
| Br$_{18}$ | 1.33 | 83.74 | 521 |
| Br$_{19}$ | 1.2 | 77.31 | 587 |
| K band | | | |
| Br$\gamma$ | 6.2 | 121.38 | 244 |

**Notes.** Positive EW indicate emission features. The EW are in Å, Fl are in unit of $10^{-13}$ erg cm$^{-2}$ s$^{-1}$ Å$^{-1}$, and FWHM are in km s$^{-1}$.

range for each T$_{\text{eff}}$ interval. Then, we measured the theoretical EWs of the H lines.

We checked if the theoretical EWs are in good agreement with those previously reported for B stars. For the Pa$\beta$ lines we made a fitting of the T$_{\text{eff}}$ versus EW behaviour using the values reported by Wallace et al. (2000) (Fig. 3 a), and compared it with the EW from the synthetic spectra (Fig. 3 b). The fitting was done using an implementation of the non-linear least-squares (NLLS) provided by GNUPLOT. In a similar way, Fig. 3 c presents the reported values of the EW of Br11 line from Meyer et al. (1998) for OB stars with luminosity classes V-III, and the comparison is in Fig. 3 d. Using a bigger sample from the APOGEE-2 DR14 catalogue (Abolfathi et al. 2018), Ramírez-Preciado et al. (2020) found a linear relationship between the sum of the EWs of the Br11 and Br13 lines and T$_{\text{eff}}$. This relationship, which is shown by a solid line in Fig. 3 e, falls in the upper limit of the theoretical EW values for stars with T$_{\text{eff}}$ in the 10 000 − 20 000 K range.

In the case of the Br$\gamma$ line, we used a fitting obtained from the measurements given by Hanson et al. (1996) (Figs. 3 f and g). Figures 3 h, i and j present the comparison of the EWs from the synthetic spectra with the fittings given by Lenorzer et al. (2002b). These fittings that give the relationship between the spectral type and the EW of some Brackett and Pfund lines were obtained empirically from a sample of 15 B-type dwarf to giant stars.

In general, we observe that the EWs obtained from the synthetic spectra are in good agreement with the values previously reported, especially in the T$_{\text{eff}}$ and log $g$ ranges typically observed in Be stars (20 000−30 000 K, 3.5−4.5 dex, e.g. Cochetti et al. 2020). Then, we used the theoretical EWs to correct the observed H lines in our sample.
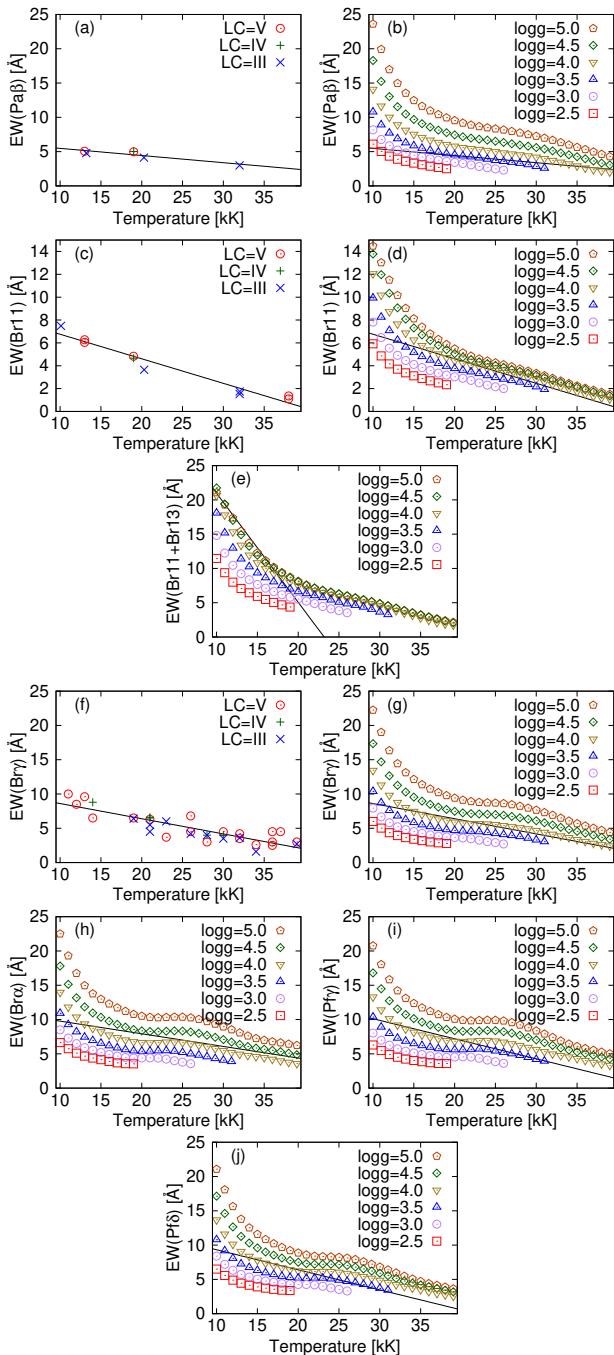
**Fig. 3.** Comparison between EW obtained through sʏɴsᴘᴇᴄ's spectra and values/fits from the literature (see Sec. 3.1 for details).

**Table 6.** Group classification of our star sample according to Mennickent's criterion.

| Group I | Group II | Group III |
|---------|----------|-----------|
| BK Cam | $\Psi_{01}$ Ori* | 66 Oph |
| 12 Vul | 228 Eri* | |
| 28 Cyg | 105 Tau | |
| V696 Mon | 120 Tau* | |
| | V1150 Tau* | |
| | 48 Per | |
| | $\omega$ Ori | |
| | EW Lac | |
| | V923 Aql | |
| | 28 Tau | |

* Reclassified to group I (see Sec.4.1).
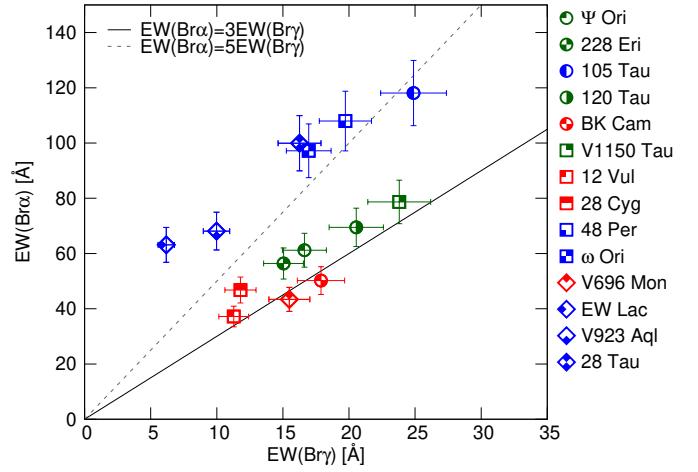


**Fig. 4.** EW(Brα) versus EW(Brγ). Red symbols are for group I stars, group II stars are plotted in blue, and green symbols are for the intermediate group I-II. The relations EW(Brα)=3 EW(Brγ) and EW(Brα)=5 EW(Brγ) are plotted in continuous and dashed lines, respectively.

### 3.3. EW(Brα)/EW(Brγ) ratio

According to the star sample analysed by Granada et al. (2010), group I objects present Brα and Brγ lines with similar EW values up to EW(Brα)≃3 EW(Brγ), while for stars in group II, the EW(Brα) is much larger (more than five times) than the EW(Brγ). This behaviour is characteristic of the optically thick models, which predict a strong depression in the emission of Brα (Lynch et al. 2000).

In Fig. 4 we plot EW(Brα) versus EW(Brγ) for the programme's stars. Each star is represented with a different symbol. The empirical limits EW(Brα)=3 EW(Brγ) and EW(Brα)=5 EW(Brγ) are plotted in continuous and dashed lines, respectively, as a reference. Group I stars, which follow the same trend as the sample of Granada et al. (2010), are plotted in red. Group II stars are plotted in blue or green symbols according to the following criterion: those which follow the trend from Granada et al. (2010) EW(Brα)≳5 EW(Brγ) are plotted in blue, and those with the EW(Brα)/EW(Brγ) ratio similar to group I stars are plotted in green. We identify the green-symbol stars as group I-II. It is worth mentioning that 28 Cyg presents an EW(Brα)/EW(Brγ) ratio a little higher than expected for a group I object.

### 3.2. Group classification

Mennickent et al. (2009) proposed a criterion to classify the Be stars into three groups, based on the relative intensity of the hydrogen emission lines observed in the L band. Group I encompasses stars with Brα and Pfγ lines with similar intensities to Humphreys lines. Stars with Brα and Pfγ lines more intense than Humphreys lines belong to group II, while group III comprises stars with no emission lines. Following this criterion, we classified the stars of our sample with L-band observations (see Figs. 2 and A.4) in the groups of Table 6.

## 3.4. Location in the Lenorzer diagram and other flux-ratio diagrams

For a dense gas, lines are optically thick and their line strengths only depend on the emitting surface. On the contrary, for low gas densities, the lines are optically thin and can be represented by Menzel's case B recombination (Baker & Menzel 1938). Lenorzer et al. (2002a) made a diagram of the flux ratios Hu14/Brα versus Hu14/Pfγ and plotted the location of different objects, together with the optically thick and optically thin limits. On this diagram, LBVs, Be, and B[e] stars are located in different loci along the diagonal between the optically thick and optically thin cases: LBVs are located in the lower part, close to the optically thin limit at $(\log(\mathrm{Fl(Hu14)/Fl(Pf\gamma)}),$ $\log(\mathrm{Fl(Hu14)/Fl(Br\alpha)})) \simeq (-0.9, -1.6)$, Be stars are close to the optically thick case at $(\log(\mathrm{Fl(Hu14)/Fl(Pf\gamma)}),$ $\log(\mathrm{Fl(Hu14)/Fl(Br\alpha)})) \simeq (0,0)$ in the upper part, while B[e] stars are in the central part. Moreover, Mennickent et al. (2009) located group I and II stars in a Lenorzer diagram and found that the group I stars are located in the top right part of the Lenorzer diagram, pointing out a compact and dense disc structure, while group II stars are more spread out and located in regions of moderate-to-small-line optical depths. Thereby, the location of the objects in the diagram gives us information about the density of the emitting gas.

Figure 5 a shows the Lenorzer diagram for those programme stars observed in the L band. The colour of the symbols in this figure is the same as in Fig 4. Stars of group I (BK Cam, 12 Vul, 28 Cyg, and V696 Mon) are located in the region $\log(\mathrm{Fl(Hu14)/Fl(Br\alpha)}) \geq -0.25$ (limit marked with a solid black line), value that is close to the limit of -0.2 adopted by Mennickent et al. (2009) for stars in this group. For stars with $\log(\mathrm{Fl(Hu14)/Fl(Br\alpha)})$ below this value, classified as belonging to group II according to the intensity of Humphreys lines, we can distinguish between the ones that present EW(Brα)/EW(Brγ) in the range expected for group II stars, and those with values nearer to the ones expected for stars of group I. Stars with EW(Brα)/EW(Brγ) ratios in the expected range for group II stars (105 Tau, 48 Per, ω Ori, EW Lac, V923 Aql, and 28 Tau) are below the limit $\log(\mathrm{Fl(Hu14)/Fl(Br\alpha)}) = -0.5$ (dashed blue line). The others, which are those that present EW(Brα)/EW(Brγ) ratios similar to those expected for group I ($\Psi_{01}$ Ori, 228 Eri, 120 Tau, and V1150 Tau), are located in the intermediate region $-0.5 \leq \log(\mathrm{Fl(Hu14)/Fl(Br\alpha)}) \leq -0.25$.

Granada et al. (2010) made a diagram similar to that of Persson & McGregor (1985) based on the Brα, Pfγ, and Brγ lines. They reported that these lines are also useful for distinguishing between compact thick or extended thin envelopes. Figure 5 b presents this diagram for our star sample, where stars of group I and I-II are located in the left part, while those of group II are located in the right part.

As observations in the L band are more difficult to obtain and both previously shown diagrams use lines from this band, we consider it useful to make a new diagram only based on lines from J, H, and K bands. With this aim, we made the diagrams shown in Figs. 5 c and d, which use the Pf18 - Brγ - Paβ and Br12 - Paβ - Brγ lines, respectively. The stars plotted in grey are those without an L-band spectrum and, therefore, without group classification and not plotted in Figs. 5 a and b.

The distributions obtained for the diagrams based on Pf18 - Brγ - Paβ and Br12 - Paβ - Brγ lines are similar to the one observed in the Lenorzer diagram. The group II stars are close to the optically thin limit in the lower part of the diagram at $(\log(\mathrm{Fl(Pf18)/Fl(Br\gamma)}),$

$\log(\mathrm{Fl(Pf18)/Fl(Pa\beta)})) \simeq (-1.4, -2.1)$ and $(\log(\mathrm{Fl(Br12)/Fl(Pa\beta)}),$ $\log(\mathrm{Fl(Br12)/Fl(Br\gamma)})) \simeq (-1.25, -0.6)$, while the group I stars are in the opposite corner, close to the optically thick case located at $(\log(\mathrm{Fl(Pf18)/Fl(Br\gamma)}), \log(\mathrm{Fl(Pf18)/Fl(Pa\beta)})) \simeq (-0.25, -0.6)$ and $(\log(\mathrm{Fl(Br12)/Fl(Pa\beta)}),$ $\log(\mathrm{Fl(Br12)/Fl(Br\gamma)})) \simeq (-0.2, -0.25)$. The location of stars in group I-II is similar to that of stars in group I, and there is one star (105 Tau) classified as group II that falls in the upper region of the Pf18 - Brγ - Paβ diagram. It is worth mentioning that the position of 105 Tau in the Lenorzer diagram is over the line that divides the group II and I-II regions, so its location in Fig. 5 c suggests that it is likely an object belonging to group I-II. This intermediate classification may also indicate that these objects are in a transition stage between groups.

For the stars without group classification, there are three (π Aqr, 48 Lib and o Aqr) that are in the middle of the gap that separates the groups in Fig. 5 c and are located in a region compatible with group II in Fig. 5 d. V1075 Sco is located in the same region in Fig. 5 d. Thus, these four stars are likely part of group II.

Regarding the other two stars, in Fig. 5 d MX Pup is in a region compatible with group I stars, while V4024 Sgr falls in an intermediate locus. Based on that, MX Pup likely belongs to group I, and we can not assign a group for V4024 Sgr.

## 3.5. Helium and metallic lines

We identify lines from He I, C I, N I, O I, Na I, Mg I, Mg II, Si I, Fe I, and Fe II. In Tables C.1 to C.3, we present the EWs of the identified lines. As we mentioned before, positive EW indicate emission features, while negative EW indicate absorption features.

He I lines are present in 18 stars of our sample, generally in absorption, with the exception of the He I line at $\lambda 2.0587\,\mu m$ which is in emission. The Fe I and Fe II lines are observed in emission in 16 and in 13 stars observed in the H band, respectively. In some of the stars that present Fe II lines in emission in the H band, Fe II lines are also observed in emission in the K and L bands. For the 19 objects observed in the J band, 15 stars present emission lines of O I, and 14 stars present C I in emission. Both elements also appear in the H- and L bands. Mg II doublet $\lambda\lambda 2.1375 - 2.1438\,\mu m$ is observed in 11 stars of the sample, while the other doublet in $\lambda\lambda 2.4038 - 2.4131\,\mu m$ is more difficult to distinguish, because it is blended with H lines. Mg II is also observed in the H band. In the H band, only five objects present N I emission at $\lambda 1.5586\,\mu m$, while four present emission from Si I $\lambda 1.5964\,\mu m$ and $\lambda 1.6064\,\mu m$. Two objects show Na I $\lambda 2.2062\,\mu m$ and $\lambda 2.2090\,\mu m$ in emission in the K band.

# 4. Discussion

## 4.1. An improved criterion to classify Be stars according to the disc opacity

Mennickent et al. (2009)'s criterion provides an easy way to separate stars in groups I and II through a qualitative description of the L-band spectrum of the Be stars, and thus to obtain information about the density of the emitting gas. However, in some cases where the Humphreys lines are quite intense, but not as intense as the Brα and Pfγ lines, the classification may be ambiguous. In fact, we see that some stars classified as group II objects based on this criterion, actually have EWs and line-flux ratios similar to the ones of group I stars. Thus, we propose that the stars in our group I-II are indeed part of group I.
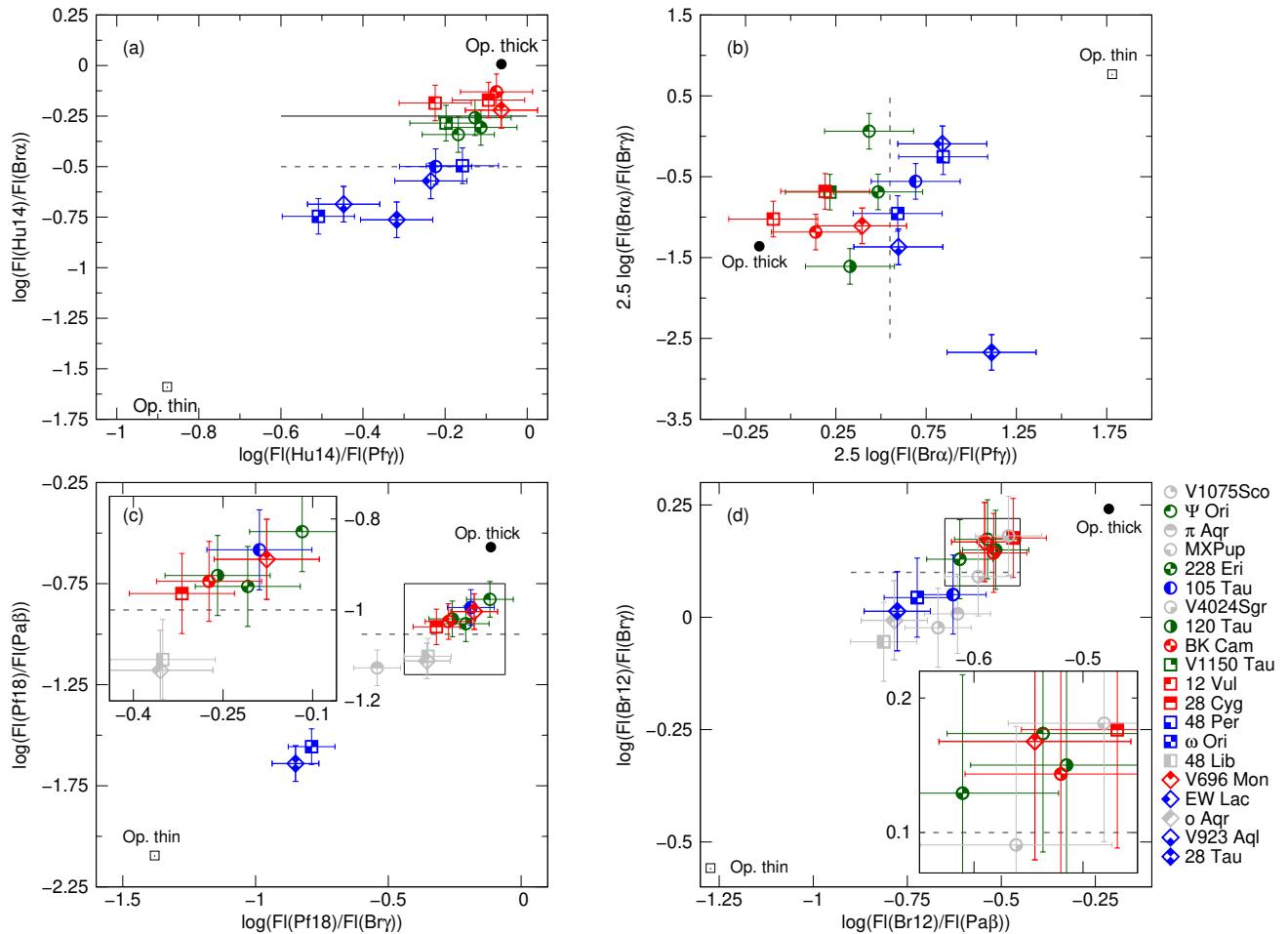
**Fig. 5.** Flux-ratio diagrams based on the following lines: (a) Hu14 - Pf$\gamma$ - Br$\alpha$ (Lenorzer's); (b) Br$\alpha$ - Pf$\gamma$ - Br$\gamma$ (Granada's - Persson & McGregor's); (c) Pf18 - Br$\gamma$ - Pa$\beta$; (d) Br12 - Pa$\beta$ - Br$\gamma$. The symbols for each star are the same as in Fig. 4, but the colour represents the group the star belongs to: red symbols represent group I stars, blue symbols group II stars, and green symbols the transition group I-II. The grey symbols are for those stars without an L-band spectrum and no group classification. Zoomed-in views of the region where symbols overlap are plotted in panels (c) and (d).

Assuming that stars in group I-II are actually part of group I, we can then quantitatively define different criteria that separate stars between groups I and II. These criteria, with limits represented by a dashed grey line in each panel of Fig. 5, are shown in Table 7. The criteria were empirically defined based on how the stars of each group gather in the different diagrams, separating group I objects from most group II objects. In Fig. 5 c, the unclassified objects laid in the gap between the group I and group II regions. Therefore, we used the information provided by Fig. 5 d, where the same unclassified objects are in positions compatible with group II membership. In Fig. 5 d, the limit could be a little displaced, because it is the only diagram where we can plot the unclassified object that is in the gap (V4024 Sgr).

With these new criteria, we can classify five of the seven stars without L-band observations. MX Pup is member of group I, while V1075 Sco, $\pi$ Aqr, 48 Lib, and $o$ Aqr are members of group II. We can also classify HD 171623 as a member of group III due to the absence of notorious emission. V4024 Sgr remains without classification because of its intermediate location in the Br12 - Pa$\beta$ - Br$\gamma$ area.

The final group classification for our sample is the following. Group I includes $\psi_{01}$ Ori, MX Pup, 228 Eri, 120 Tau, BK Cam, V1150 Tau, 12 Vul, 28 Cyg, and V696 Mon; Group II includes V1075 Sco, $\pi$ Aqr, 105 Tau, 48 Per, $\omega$ Ori, 48 Lib, EW Lac,

**Table 7.** Quantitative criteria to classify stars in groups I and II, according to limits set on Fig. 5.

| Ratio | Group I | Group II |
|---|---|---|
| log(Fl(Hu14)/Fl(Br$\alpha$)) | $\gtrsim -0.5$ | $\lesssim -0.5$ |
| 2.5·log(Fl(Br$\alpha$)/Fl(Pf$\gamma$)) | $\lesssim 0.55$ | $\gtrsim 0.55$ |
| log(Fl(Pf18)/Fl(Pa$\beta$)) | $\gtrsim -1$ | $\lesssim -1$ |
| log(Fl(Br12)/Fl(Br$\gamma$)) | $\gtrsim 0.1$ | $\lesssim 0.1$ |

$o$ Aqr, V923 Aql, and 28 Tau; Group III includes 66 Oph and HD 171623. V4024 Sgr remains unclassified.

It is worth highlighting that the nine stars that belong to group I have $T_{eff} \geq 18000$, while seven of the ten stars in group II have $T_{eff} \leq 18000$. The three stars in group II with $T_{eff} \geq 18000$ are 105 Tau, for which we mentioned its limit position in the Lenorzer's diagram, $\pi$ Aqr and V1075 Sco. This agrees with the result achieved by Sabogal et al. (2017), who mentioned that late Be stars present more tenuous and optically thin discs than early-type Be stars, but some early-type stars could present optically thin discs when they lose their discs.
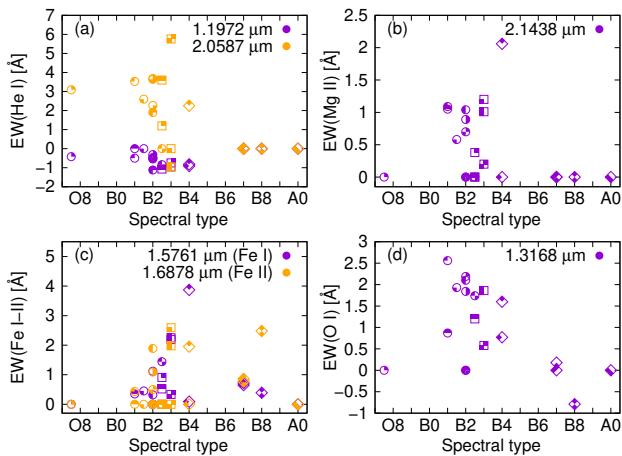
**Fig. 6.** EW versus ST for representative lines of He I, Mg II, Fe I, Fe II and O I. The uncertainties for the EWs are around 10% of the values.



**Fig. 7.** FWHMs of Br10 (a), Br$\delta$ (b), Hu14 (c), and Br$\alpha$ (d) lines versus $V \sin i$. Linear fits (red line) and 95% confidence intervals (grey area) are superimposed in each panel.

### 4.2. Behaviour of the He and metallic lines

Figure 6 shows the EWs of representative lines from different elements versus the spectral type of the star. The symbols are the same as in Fig. 4, but different colours represent different lines of the same element, as is indicated in each panel.

In Fig. 6 a, we plot the EW values from the He I $\lambda 2.0587 \,\mu m$ line in emission and the He I $\lambda 1.1972 \,\mu m$ line in absorption. The He I is observed only in early B-type stars, with EW Lac (ST B4) and V696 Mon (ST B3-5) being the stars with the latest spectral type that present this element. This is in good agreement with previous results by Hanson et al. (1996), Clark & Steele (2000) and Lenorzer et al. (2002b).

The Mg II $\lambda 2.1438 \,\mu m$ line is only observed in the same spectral types as He lines (see Fig. 6 b). This agrees with the results by Clark & Steele (2000), who said that Mg II lines are likely excited via Ly$\beta$ fluorescence (Bowen 1947) and are observed in stars with spectral types earlier than B4.

Regarding Fe I $\lambda 1.5761 \,\mu m$ and Fe II $\lambda 1.6878 \,\mu m$ lines (Fig. 6 c), it seems that the emission is maximum for spectral types B2-B4. Through the comparison between the EWs of Fe II, Mg II and Br$\gamma$, Clark & Steele (2000) proposed that neither Fe II nor Mg II lines are seen in emission when EW(Br$\gamma$)< 8 Å. We only have one object with EW(Br$\gamma$)< 8 Å (EW Lac), which does not present Fe II or Mg II emission in the K band.

Lenorzer et al. (2002b) reported that O I emission lines in the L band are observed in Be stars earlier than B3. However, in the K band we observe O I $\lambda 1.3168 \,\mu m$ emission lines in stars with spectral types up to B7. It is worth mentioning that, as is shown in Fig. 6 d, the EW of O I emission lines becomes smaller for later spectral-type objects. This relation could be useful to estimate the ST of the star. In all the cases, EW(1.3168 $\mu m$)/EW(1.129 $\mu m$)<1, as is expected if the Ly$\beta$ fluorescence process has a significant role in the excitation of the O I lines.

For the C I $\lambda 1.1756 \,\mu m$ line, the existence of a correlation is not clear. Clark & Steele (2000) mentioned that the presence of Na I emission features suggests that a region of the circumstellar envelope should be shielded from direct stellar radiation, due to the low ionisation energy. This could be the case for 48 Per and V696 Mon, which are the two objects of our sample that present emission in Na I lines in the K band.
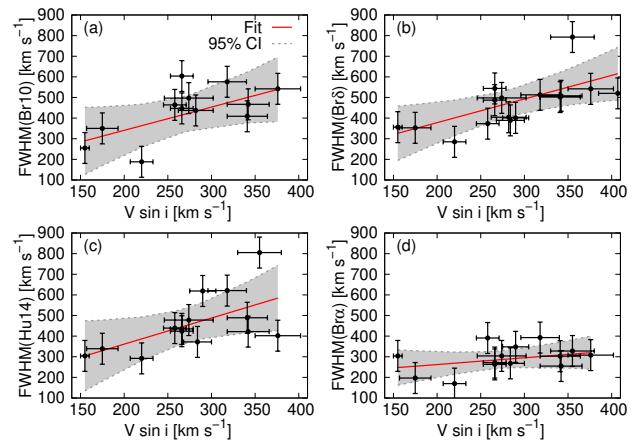
### 4.3. Correlation with $V \sin i$

To discuss if the main mechanism of broadening is rotational, we analyse the correlation between the FWHM and $\Delta$V parameters versus $V \sin i$. A strong correlation between the FWHM and $V \sin i$ was found by Hanuschik (1989) for optical lines and Granada et al. (2010) for IR lines.

The determination of the FWHM and $\Delta$V depends on the spectral resolution; therefore, to analyse their correlation with $V \sin i$ we selected GNIRS spectra. These spectra have the same resolution, and the sample is bigger than that observed with FIRE.

In Fig. 7, we plot the FWHM values of the Br10, Br$\delta$, Hu14, and Br$\alpha$ lines versus $V \sin i$. In each panel, a linear fitting and the 95% confidence interval are superimposed with a red line and grey area. To quantify the statistical relationship between the FWHM and $V \sin i$, we calculated the Pearson correlation coefficient for the distributions. For Br10, Br$\delta$, and Hu14 lines (Figs. 7 a, b, and c) we found a strong correlation with Pearson's coefficients of 0.65, 0.67, and 0.60, respectively. Contrary to Granada et al. (2010), we found no correlation between the FWHM versus $V \sin i$ for the lines Pf$\gamma$ and Br$\alpha$ (see Fig. 7 d), nor for Br$\gamma$, Pa $\alpha$, Pa$\beta$, or Pf$\delta$ lines.

Figure 8 presents the peak separation versus $V \sin i$ for the same lines that the FWHM correlates with $V \sin i$ (Br10, Br$\delta$ and Hu14). It is seen that the $\Delta$V values on the Br10 line follow the relationship $\Delta$V = $V \sin i$, which is plotted via a in dashed blue line. For the Hu14 line, the correlation is weaker, and there is no correlation for the Br$\delta$ line.

It is worth mentioning that those FWHMs and $\Delta$V that better correlate to $V \sin i$ correspond to higher-order Humphreys and Brackett lines, which form in inner parts of the disc compared the low-order lines (Hony et al. 2000; Mennickent et al. 2009), which form in outer parts. So, these lines might be useful when estimating the $V \sin i$ of the stars.

## 5. Conclusions

The IR spectra of Be stars are excellent sources of information on the physical and dynamical structure of different regions inside the disc. Their analysis contributes to a better understanding of the possible mechanism involved in the development and evolution of the disc. However, a great number of NIR spectra and a wide spectral range coverage are required to attain a more complete overview of the Be phenomenon.
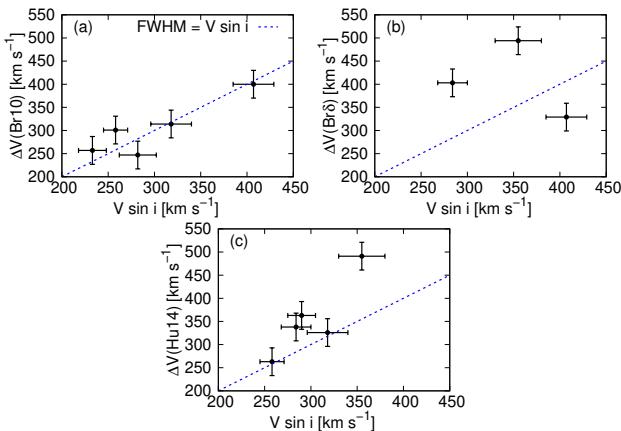
**Fig. 8.** Peak separation of the Br10 (a), Br$\delta$ (b) and Hu14 (c) lines versus $V \sin i$. The linear relation $\Delta V = V \sin i$ is represented by a dashed blue line.

With this aim, we present an atlas of quasi simultaneous J-, H-, K-, and L-band observations of a sample of 22 Be stars obtained with the GNIRS and FIRE spectrographs. We identify several lines of the Paschen, Brackett, Pfund and Humphreys series of hydrogen. Lines of He I, C I, N I, O I, Na I, Mg I, Mg II, Si I, Fe I, and Fe II are also identified.

He I lines are observed in early B-type stars. In the same spectral types, the Mg II and O I lines are observed in emission. Moreover, we report that the intensity of the O I $\lambda 1.3168\,\mu m$ emission line decreases towards the later spectral types. This reveals the importance of the Ly$\beta$ fluorescence process on Mg II and O I transitions.

We also find a correlation between the FWHM of the Br10, Br$\delta$, and Hu14 lines with $V \sin i$. This indicates that the broadening mechanism is mainly rotational. In addition, the peak separation of Br10 line correlates strongly with $V \sin i$, while the correlation is weaker for the Hu14 line. We thus propose that these lines are useful when estimating the projected rotational velocity of Be stars.

Through the analysis of different hydrogen line-flux ratio diagrams, and taking into account the different value ranges from the EW(Br$\alpha$)/EW(Br$\gamma$) ratio, we propose new criteria to classify the Be stars into Mennickent's groups. These new criteria also allow us to unify the classification that comes from previous works, which are the definition of the groups given by Mennickent et al. (2009) and the location of the different groups on Lenorzer's diagram reported by Granada et al. (2010). Moreover, the new criteria involve lines not only in the L band, which are more difficult to obtain, but also in the J, H, and K bands. Using these criteria, we can identify some objects that present compact thick envelopes in our sample (group I stars: $\psi_{01}$ Ori, MX Pup, 228 Eri, 120 Tau, BK Cam, V1150 Tau, 12 Vul, 28 Cyg and V696 Mon), while in others the envelope is extended and optically thin (group II stars: V1075 Sco, $\pi$ Aqr, 105 Tau, 48 Per, $\omega$ Ori, 48 Lib, EW Lac, $o$ Aqr, V923 Aql and 28 Tau). The presence of an optically thin or thick disc seems to depend on $T_{\rm eff}$, since group I stars have $T_{\rm eff} \geq 18000$ while most group II stars have $T_{\rm eff} \leq 18000$. We also find two objects that do not present an emitting disc at the observing time (66 Oph and HD 171623), and one star (V4024 Sgr) remains unclassified.

Paper II of this series will use the line parameters from this work to obtain a characterisation of the envelopes. It could be valuable to discuss the evolution of the envelopes through the analysis of the variability of their physical conditions and to identify some peculiar objects such as 12 Vul, which has presented a transitory $^{12}$CO emission (Cochetti et al. 2021). A better knowledge of the properties and evolution of the envelopes enable us to set constraints on the theoretical models of the stars with the Be phenomenon.

# References

Abolfathi, B., Aguado, D. S., Aguilar, G., et al. 2018, ApJS, 235, 42
Abt, H. A., Levato, H., & Grosso, M. 2002, ApJ, 573, 359
Baker, J. G. & Menzel, D. H. 1938, ApJ, 88, 52
Bowen, I. S. 1947, PASP, 59, 196
Chauville, J., Zorec, J., Ballereau, D., et al. 2001, A&A, 378, 861
Chojnowski, S. D., Whelan, D. G., d, J. P., et al. 2015, AJ, 149, 7
Chojnowski, S. D., Wisniewski, J. P., Whelan, D. G., et al. 2017, AJ, 153, 174
Clark, J. S. & Steele, I. A. 2000, A&AS, 141, 65
Cochetti, Y. R., Arcos, C., Kanaan, S., et al. 2019, A&A, 621, A123
Cochetti, Y. R., Arias, M. L., Kraus, M., et al. 2021, A&A, 647, A164
Cochetti, Y. R., Zorec, J., Cidale, L. S., et al. 2020, A&A, 634, A18
Collins, II, G. W. 1987, in IAU Colloq. 92: Physics of Be Stars, ed. A. Slettebak & T. P. Snow, 3–19
Cox, A. N. & Pilachowski, C. A. 2000, Physics Today, 53, 77
Elias, J. H., Joyce, R. R., Liang, M., et al. 2006a, in Society of Photo-Optical Instrumentation Engineers (SPIE) Conference Series, Vol. 6269, Society of Photo-Optical Instrumentation Engineers (SPIE) Conference Series, ed. I. S. McLean & M. Iye, 62694C
Elias, J. H., Rodgers, B., Joyce, R. R., et al. 2006b, in Society of Photo-Optical Instrumentation Engineers (SPIE) Conference Series, Vol. 6269, Society of Photo-Optical Instrumentation Engineers (SPIE) Conference Series, ed. I. S. McLean & M. Iye, 626914
Frémat, Y., Zorec, J., Hubert, A.-M., & Floquet, M. 2005, A&A, 440, 305
Głębocki, R. & Gnaciński, P. 2005, in ESA Special Publication, Vol. 560, 13th Cambridge Workshop on Cool Stars, Stellar Systems and the Sun, ed. F. Favata, G. A. J. Hussain, & B. Battrick, 571
Granada, A., Arias, M. L., & Cidale, L. S. 2010, AJ, 139, 1983
Hanson, M. M., Conti, P. S., & Rieke, M. J. 1996, ApJS, 107, 281
Hanuschik, R. W. 1989, Ap&SS, 161, 61
Hony, S., Waters, L. B. F. M., Zaal, P. A., et al. 2000, A&A, 355, 187
Hubeny, I. 1988, Computer Physics Communications, 52, 103
Hubeny, I. & Lanz, T. 1995, ApJ, 439, 875
Hubeny, I. & Lanz, T. 2011, Synspec: General Spectrum Synthesis Program, Astrophysics Source Code Library
Hubeny, I. & Lanz, T. 2017, arXiv e-prints [arXiv:1706.01859]
Hubert, A. M. & Floquet, M. 1998, A&A, 335, 565
Jaschek, M., Slettebak, A., & Jaschek, C. 1981, Be star terminology., be Star Newsletter
Kurucz, R. L. 1979, ApJS, 40, 1
Lenorzer, A., de Koter, A., & Waters, L. B. F. M. 2002a, A&A, 386, L5
Lenorzer, A., Vandenbussche, B., Morris, P., et al. 2002b, A&A, 384, 473
Lynch, D. K., Rudy, R. J., Mazuk, S., & Puetter, R. C. 2000, ApJ, 541, 791
Mathew, B., Banerjee, D. P. K., Naik, S., & Ashok, N. M. 2012a, MNRAS, 423, 2486
Mathew, B., Banerjee, D. P. K., Subramaniam, A., & Ashok, N. M. 2012b, ApJ, 753, 13
Mennickent, R. E., Sabogal, B., Granada, A., & Cidale, L. 2009, PASP, 121, 125
Meyer, M. R., Edwards, S., Hinkle, K. H., & Strom, S. E. 1998, ApJ, 508, 397
Persson, S. E. & McGregor, P. J. 1985, AJ, 90, 1860
Ramírez-Preciado, V. G., Roman-Lopes, A., Román-Zúñiga, C. G., et al. 2020, ApJ, 894, 5
Rivinius, T., Carciofi, A. C., & Martayan, C. 2013, A&A Rev., 21, 69
Sabogal, B. E., Ubaque, K. Y., García-Varela, A., Álvarez, M., & Salas, L. 2017, PASP, 129, 014203
Steele, I. A. & Clark, J. S. 2001, A&A, 371, 643
Štefl, S., Rivinius, T., Carciofi, A. C., et al. 2009, A&A, 504, 929
Wallace, L., Meyer, M. R., Hinkle, K., & Edwards, S. 2000, ApJ, 535, 325
Zorec, J., Frémat, Y., & Cidale, L. 2005, A&A, 441, 235

## Appendix A: Spectra of the star sample
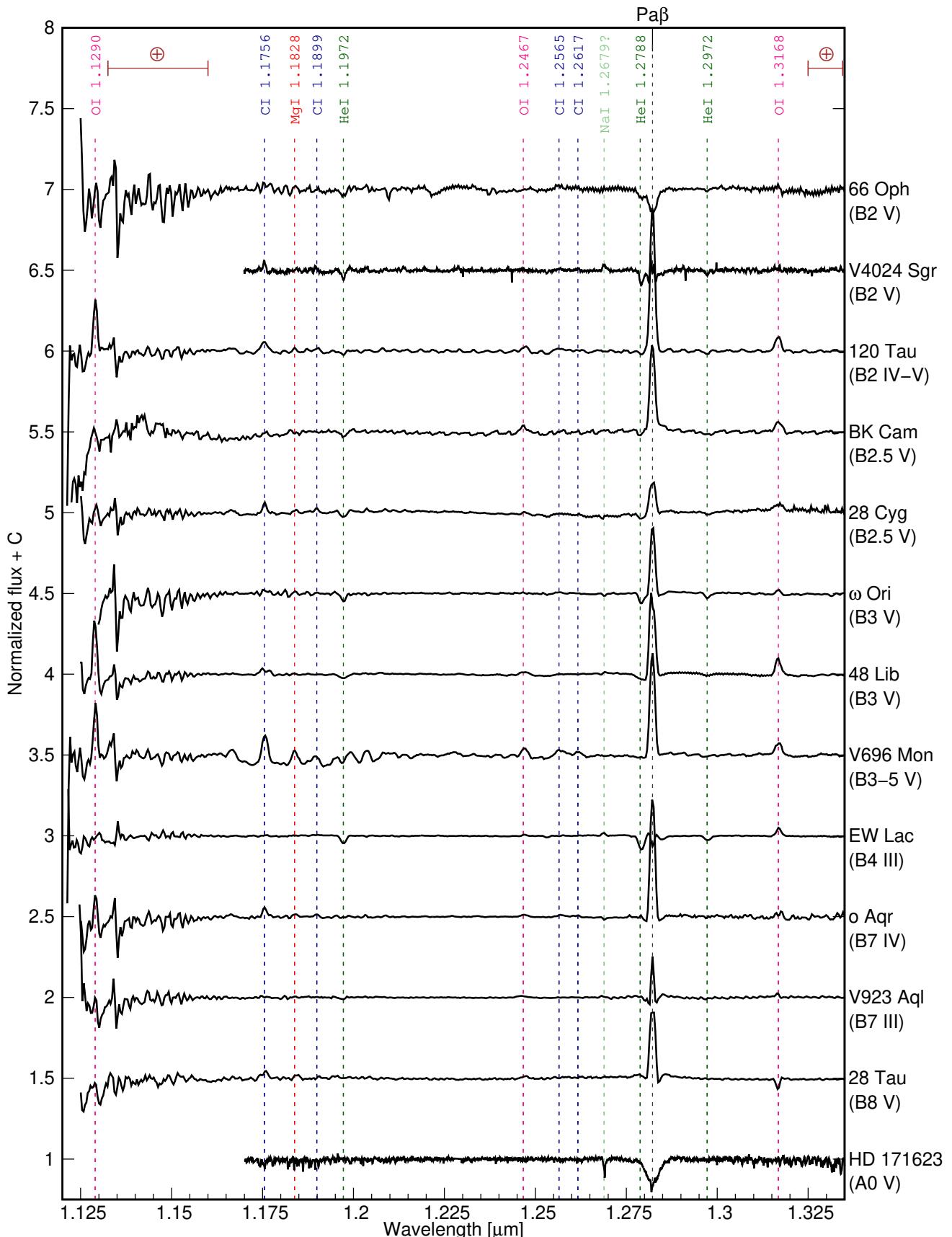


**Fig. A.1.** J-Band spectra of Be stars. Spectra are normalised and shifted vertically to ease comparison.
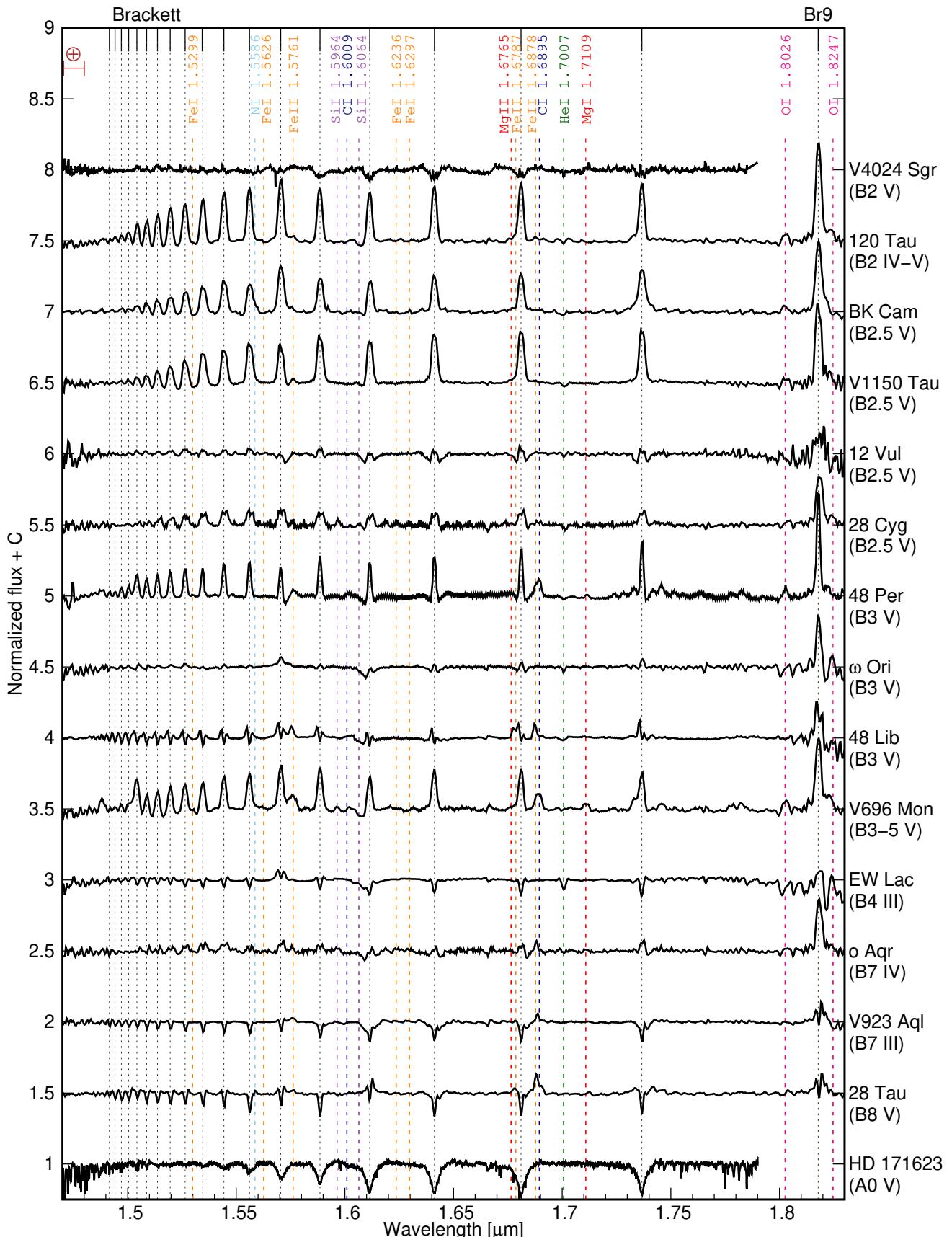
**Fig. A.2.** H-band spectra of Be stars. Spectra are normalised and shifted vertically to ease comparison.
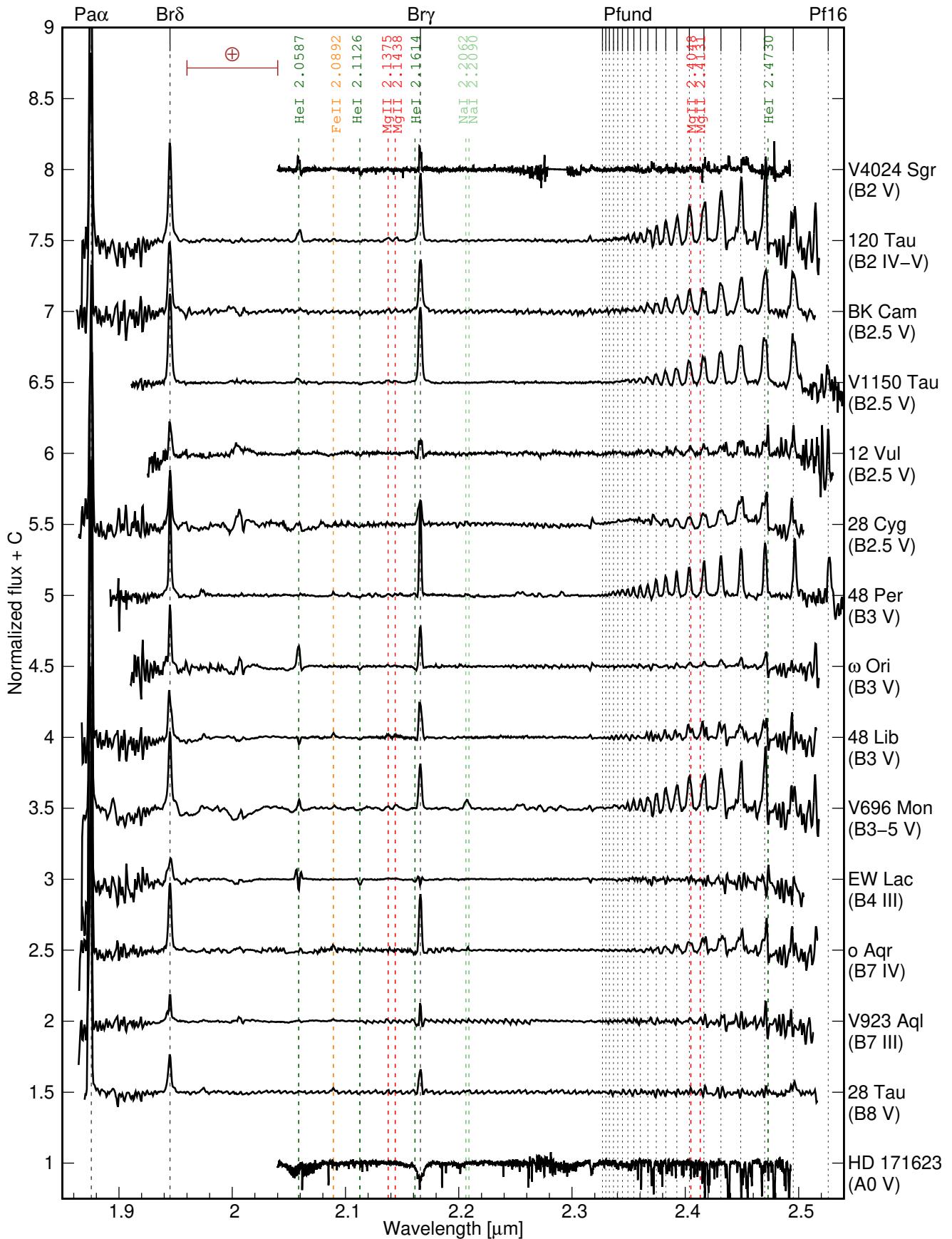
**Fig. A.3.** K-band spectra of Be stars. Spectra are normalised and shifted vertically to ease comparison.
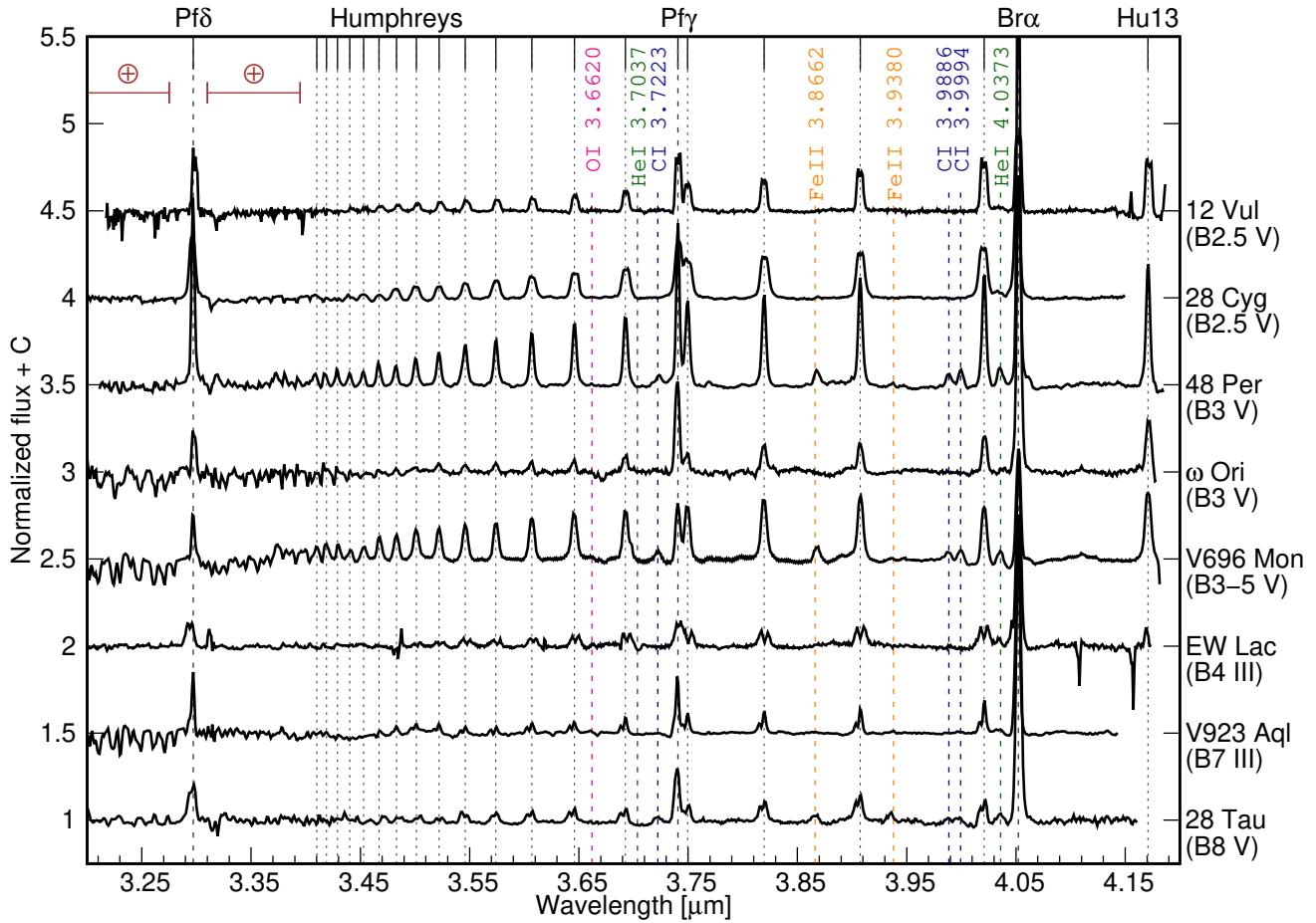
**Fig. A.4.** L-band spectra of Be stars. Spectra are normalised and shifted vertically to ease comparison.



**Fig. A.5.** Paα-line profiles.

Brα
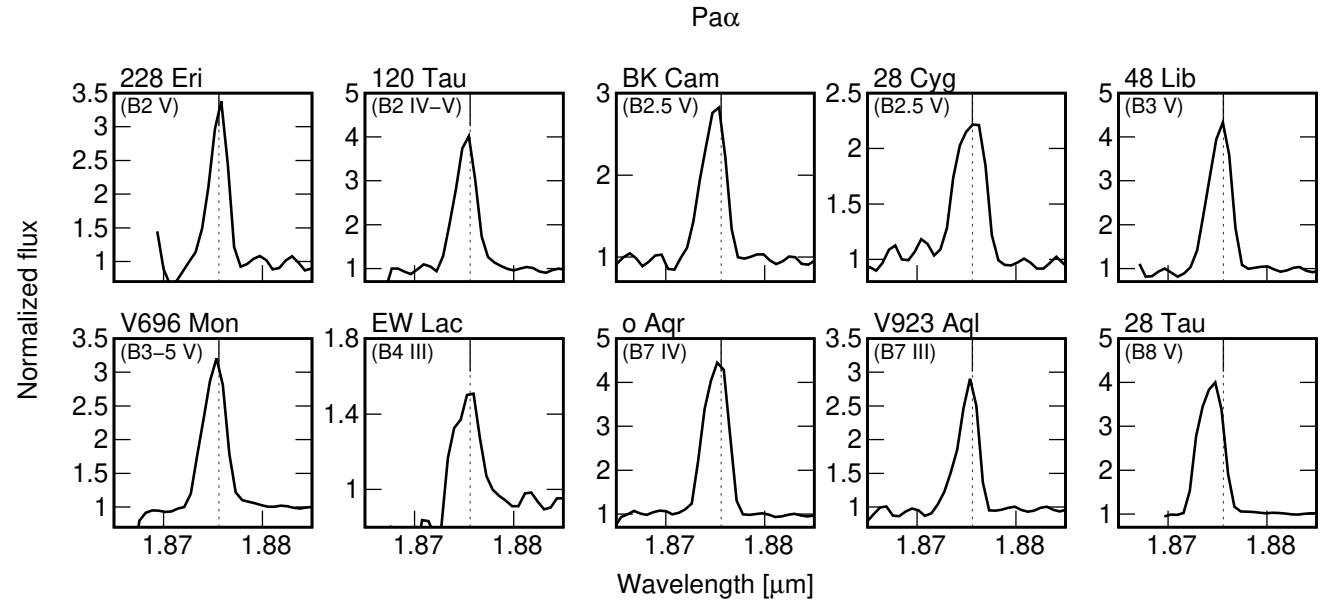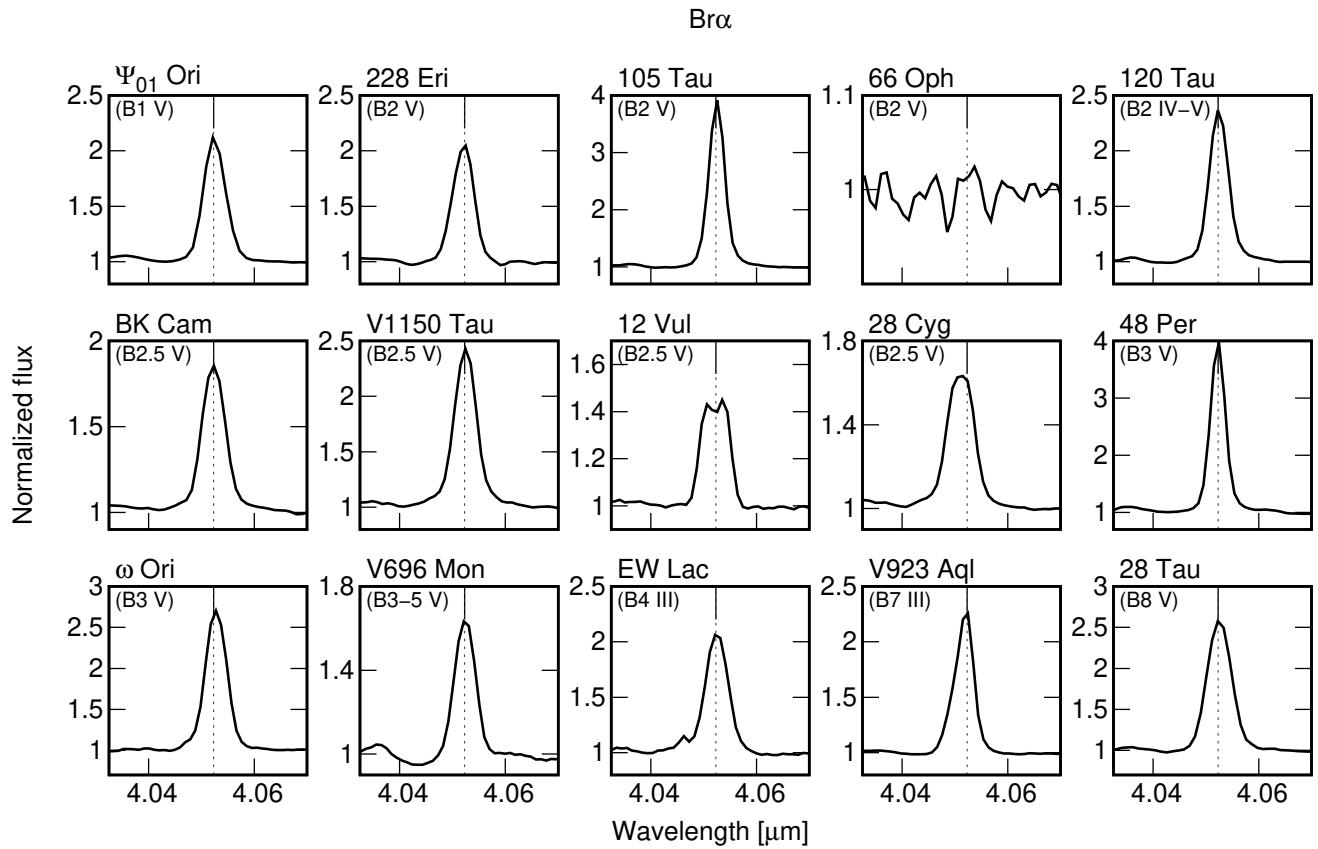


**Fig. A.6.** Brα-line profiles.

## Appendix B: H-line parameters

The following tables show the line parameters of each H line for the star sample. The EW are in Å, Fl are in units of $10^{-13}$ erg cm$^{-2}$ s$^{-1}$ Å$^{-1}$, and FWHM and $\Delta V$ are in km s$^{-1}$.

**Table B.1.** $\Psi$ Ori - EW, Fl, and FWHM of the hydrogen lines.

| Band | Line | EW | Fl | FWHM |
|------|------|-----|-----|------|
| J-Band | Pa$\beta$ | 18.66 | 529.86 | 310 |
| H-Band | Br9 | 27.89 | 312.63 | 472 |
| | Br10 | 14.82 | 173 | 604 |
| | Br11 | 13.21 | 162.21 | 524 |
| | Br12 | 11.96 | 153.98 | 507 |
| | Br13 | 10.41 | 139.14 | 475 |
| | Br14 | 11.77 | 167.43 | 587 |
| | Br15 | 12.87 | 193.56 | 608 |
| | Br16 | 10.41 | 157.97 | 622 |
| | Br17 | 9.38 | 146.95 | 608 |
| | Br18 | 7.09 | 115.71 | 562 |
| | Br19 | 6.56 | 111.16 | 511 |
| | Br20 | 5.31 | 92.45 | 509 |
| | Br21 | 3.68 | 66.3 | 477 |
| | Br22 | 2.09 | 39.02 | 393 |
| | Br23 | 1.65 | 31.41 | 341 |
| | Br24 | 0.92 | 18.03 | 341 |
| K-Band | Pf17 | | em | |
| | Pf18 | 17.49 | 78.78 | 448 |
| | Pf19 | 9.52 | 44.62 | 305 |
| | Pf20 | 12.18 | 57.09 | 560 |
| | Pf21 | 9.21 | 43.61 | 568 |
| | Pf22 | 7.37 | 35.7 | 476 |
| | Pf23 | 5.90 | 28.71 | 507 |
| | Pf24 | 4.47 | 22.05 | 423 |
| | Pf25 | 3.31 | 16.55 | 398 |
| | Pf26 | 2.10 | 10.81 | 376 |
| | Pf27 | 1.32 | 6.9 | 273 |
| | Pf28 | 0.78 | 4.12 | 188 |
| | Pf29 | 0.60 | 3.17 | 190 |
| | Br$\gamma$ | 16.63 | 103.25 | 332 |
| | Br$\delta$ | 27.16 | 234.27 | 544 |
| L-Band | Hu13 | | em | |
| | Br$\alpha$ | 61.20 | 109.37 | 272 |
| | Hu14 | 27.10 | 49.81 | 424 |
| | Hu15 | 28.62 | 55.61 | 510 |
| | Hu16 | 27.22 | 57.98 | 547 |
| | Hu17 | 23.33 | 53.96 | 540 |
| | Pf$\gamma$ | 31.46 | 73.30 | 368 |
| | Hu18 | 20.85 | 50.91 | 552 |
| | Hu19 | 16.62 | 42.98 | 530 |
| | Hu20 | 14.52 | 38.57 | 531 |
| | Hu21 | 12.36 | 33.87 | 563 |
| | Hu22 | 11.33 | 31.89 | 543 |
| | Hu23 | 9.95 | 29.03 | 527 |
| | Hu24 | 8.54 | 25.58 | 540 |
| | Hu25 | 5.91 | 18.07 | 437 |
| | Hu26 | 3.98 | 12.42 | 413 |
| | Hu27 | 2.96 | 9.35 | 491 |
| | Hu28 | 2.21 | 7.11 | 479 |
| | Hu29 | 1.67 | 5.41 | $\cdots$ |
| | Pf$\delta$ | 19.69 | 73.90 | 222 |

**Table B.2.** $\pi$ Aqr - EW, Fl, FWHM, and $\Delta V$ of the hydrogen lines.

| Band | Line | EW | Fl | FWHM | $\Delta V$ |
|------|------|-----|-----|------|-----|
| J-Band | Pa$\beta$ | 10.12 | 41.82 | 357 | 212 |
| H-Band | Br10 | 6.2 | 9.7 | $\cdots$ | 257 |
| | Br11 | 5.85 | 9.81 | $\cdots$ | 247 |
| | Br12 | 5.93 | 10.11 | 455 | 251 |
| | Br13 | 4.2 | 7.47 | 393 | 272 |
| | Br14 | 5.54 | 10.37 | 500 | 288 |
| | Br15 | 4.93 | 9.64 | 473 | 268 |
| | Br16 | 4.68 | 9.63 | 495 | 293 |
| | Br17 | 4.88 | 10.39 | 514 | 287 |
| | Br18 | 4.6 | 10.21 | 491 | 274 |
| | Br19 | 4 | 9.16 | 490 | 281 |
| | Br20 | 3.55 | 8.4 | 474 | 274 |
| | Br21 | 3.96 | 9.52 | 483 | 275 |
| | Br22 | 2.63 | 6.41 | 480 | 276 |
| | Br23 | 2.25 | 5.62 | 492 | 269 |
| K-Band | Pf17 | 8.19 | 4.67 | $\cdots$ | 250 |
| | Pf18 | 4.85 | 2.85 | $\cdots$ | 268 |
| | Pf19 | 6.73 | 3.99 | $\cdots$ | 307 |
| | Pf20 | 4.39 | 2.67 | $\cdots$ | 278 |
| | Pf21 | 6.44 | 3.94 | $\cdots$ | $\cdots$ |
| | Pf22 | 4.37 | 2.76 | $\cdots$ | $\cdots$ |
| | Pf23 | 3.69 | 2.37 | $\cdots$ | $\cdots$ |
| | Pf24 | 3.51 | 2.29 | $\cdots$ | $\cdots$ |
| | Pf25 | 3.19 | 2.11 | $\cdots$ | $\cdots$ |
| | Pf26 | 2.16 | 1.45 | $\cdots$ | $\cdots$ |
| | Pf27-28 | | em | | |
| | Br$\gamma$ | 10.51 | 9.93 | 359 | 211 |

**Table B.3.** MX Pup - EW, Fl, FWHM, and $\Delta V$ of the hydrogen lines.

| Band | Line | EW | Fl | FWHM | $\Delta V$ |
|------|------|-----|-----|------|-----|
| J-Band | Pa$\beta$ | 18.52 | 39.71 | 191 | 98 |
| H-Band | Br10 | 15.93 | 12.55 | 290 | 116 |
| | Br11 | 15.79 | 13.06 | 310 | 117 |
| | Br12 | 14.53 | 13.13 | 310 | 112 |
| | Br13 | 13.34 | 12.73 | 316 | 144 |
| | Br14 | 13.72 | 13.52 | 339 | 137 |
| | Br15 | 13.35 | 13.49 | 338 | 127 |
| | Br16 | 12.12 | 12.86 | 335 | 106 |
| | Br17 | 11.28 | 12.32 | 345 | 115 |
| | Br18 | 9.99 | 11.19 | 340 | 101 |
| | Br19 | 8.52 | 9.82 | 340 | 113 |
| | Br20 | 7.21 | 8.51 | 336 | 114 |
| | Br21 | 4.60 | 5.71 | 286 | 124 |
| | Br22 | 4.49 | 5.55 | 308 | 111 |
| | Br23 | 3.25 | 4.14 | 295 | 161 |
| | Br24 | 2.30 | 2.99 | 266 | 133 |
| | Br25 | 2.01 | 2.64 | 285 | 140 |
| | Br26 | 1.63 | 2.15 | 286 | 134 |
| | Br27 | 1.27 | 1.71 | 297 | $\cdots$ |
| | Br28-29 | | em | | |
| K-Band | Br$\gamma$ | 20.90 | 8.65 | 229 | 102 |

**Table B.4.** 228 Eri - EW, Fl, and FWHM of the hydrogen lines.

| Band | Line | EW | Fl | FWHM |
|------|------|------|------|------|
| J-Band | Paβ | 15.97 | 343.01 | 301 |
| H-Band | Br₉ | 21.98 | 130.5 | 528 |
| | Br10 | 11.17 | 85.2 | 467 |
| | Br11 | 9.92 | 83.61 | 442 |
| | Br12 | 9.35 | 84.11 | 459 |
| | Br13 | 8.14 | 77.73 | 462 |
| | Br14 | 8.78 | 88.57 | 559 |
| | Br15 | 11.07 | 115.92 | 629 |
| | Br16 | 7.08 | 76.1 | 564 |
| | Br17 | 6.56 | 72.22 | 558 |
| | Br18 | 5.70 | 64.08 | 576 |
| | Br19 | 4.86 | 55.91 | 563 |
| | Br20 | 4.27 | 50.18 | 529 |
| | Br21 | 2.88 | 34.7 | 465 |
| | Br22 | 1.80 | 22.24 | 434 |
| | Br23 | 1.27 | 16.07 | 392 |
| | Br24-26 | | em | |
| K-Band | Pf16-17 | | em | |
| | Pf18 | 17.13 | 38.64 | 463 |
| | Pf19 | 8.72 | 21.56 | 377 |
| | Pf20 | 12.39 | 30.06 | 600 |
| | Pf21 | 7.56 | 19.26 | 533 |
| | Pf22 | 6.87 | 18.19 | 483 |
| | Pf23 | 5.12 | 13.96 | 520 |
| | Pf24 | 3.98 | 11.15 | 426 |
| | Pf25 | 3.04 | 8.68 | 412 |
| | Pf26 | 2.83 | 8.26 | 622 |
| | Pf27 | 0.87 | 2.61 | ⋯ |
| | Pf28 | 1.10 | 3.28 | ⋯ |
| | Pf29 | 0.71 | 2.17 | ⋯ |
| | Pf30-31 | | em | |
| | Brγ | 15.05 | 62.45 | 321 |
| | Brδ | 22.80 | 123.95 | 508 |
| | Paα | 63.88 | 338.67 | 279 |
| L-Band | Hu13 | | em | |
| | Brα | 56.39 | 33.13 | 255 |
| | Hu14 | 26.36 | 16.36 | 422 |
| | Hu15 | 29.71 | 18.91 | 554 |
| | Hu16 | 22.87 | 16.09 | 504 |
| | Hu17 | 21.03 | 15.27 | 523 |
| | Pfγ | 29.11 | 21.21 | 362 |
| | Hu18 | 18.55 | 14.05 | 489 |
| | Hu19 | 16.04 | 12.44 | 586 |
| | Hu20 | 12.99 | 10.36 | 550 |
| | Hu21 | 12.49 | 10.05 | 613 |
| | Hu22 | 10.31 | 8.46 | 552 |
| | Hu23 | 8.60 | 7.22 | 515 |
| | Hu24 | 5.21 | 4.40 | 320 |
| | Hu25 | 6.31 | 5.32 | 434 |
| | Hu26 | 2.52 | 2.17 | 324 |
| | Pfδ | 25.98 | 28.90 | 295 |

**Table B.5.** 105 Tau - EW, Fl, and FWHM of the hydrogen lines.

| Band | Line | EW | Fl | FWHM |
|------|------|------|------|------|
| J-Band | Paβ | 27.52 | 598.77 | 217 |
| H-Band | Br₉ | 27.72 | 235.55 | 343 |
| | Br10 | 16.04 | 146.26 | 350 |
| | Br11 | 14.9 | 143.85 | 343 |
| | Br12 | 13.93 | 140.94 | 346 |
| | Br13 | 12.2 | 128.82 | 343 |
| | Br14 | 12.25 | 139.11 | 384 |
| | Br15 | 14.18 | 166.5 | 463 |
| | Br16 | 10.62 | 127.77 | 425 |
| | Br17 | 9.5 | 117.73 | 420 |
| | Br18 | 7.5 | 96.06 | 399 |
| | Br19 | 7.41 | 97.26 | 403 |
| | Br20 | 6.29 | 84.31 | 399 |
| | Br21 | 4.6 | 63.6 | 370 |
| | Br22 | 3.48 | 49.32 | 352 |
| | Br23 | 2.97 | 42.99 | 318 |
| | Br24 | 1.57 | 23.46 | ⋯ |
| | Br25 | 0.99 | 15.15 | ⋯ |
| K-Band | Pf17 | | em | |
| | Pf18 | 25.18 | 81.19 | 353 |
| | Pf19 | 13.83 | 48.22 | 275 |
| | Pf20 | 16.42 | 57.41 | 533 |
| | Pf21 | 12.8 | 45.55 | 491 |
| | Pf22 | 9.23 | 33.88 | 418 |
| | Pf23 | 7.11 | 26.51 | 420 |
| | Pf24 | 5.72 | 21.6 | 356 |
| | Pf25 | 4.51 | 17.29 | 360 |
| | Pf26 | 3.69 | 14.48 | 426 |
| | Pf27 | 2.21 | 8.83 | ⋯ |
| | Pf28 | 1.63 | 6.58 | ⋯ |
| | Pf29 | 1.02 | 4.19 | ⋯ |
| | Pf30 | 0.76 | 3.14 | ⋯ |
| | Brγ | 24.88 | 125.46 | 259 |
| | Brδ | 31.07 | 216.29 | 353 |
| L-Band | Brα | 118.11 | 75.06 | 197 |
| | Hu14 | 34.44 | 23.74 | 339 |
| | Hu15 | 32.89 | 25.28 | 372 |
| | Hu16 | 33.37 | 28.16 | 406 |
| | Hu17 | 26.61 | 24.31 | 408 |
| | Pfγ | 43.10 | 39.68 | 265 |
| | Hu18 | 18.85 | 18.53 | 347 |
| | Hu19 | 17.78 | 18.13 | 357 |
| | Hu20 | 16.44 | 17.14 | 384 |
| | Hu21 | 15.62 | 16.69 | 444 |
| | Hu22 | 13.46 | 14.96 | 459 |
| | Hu23 | 11.11 | 12.71 | 439 |
| | Hu24 | 8.96 | 10.5 | 425 |
| | Hu25 | 6.53 | 7.76 | 368 |
| | Hu26 | 5.50 | 6.65 | 396 |
| | Hu27 | 3.36 | 4.12 | ⋯ |
| | Hu28 | 2.27 | 2.83 | ⋯ |
| | Pfδ | 33.28 | 49.99 | 263 |

**Table B.6.** V4024 Sgr - EW, Fl, FWHM, and $\Delta V$ of the hydrogen lines.

| Band | Line | EW | Fl | FWHM | $\Delta V$ |
|---|---|---|---|---|---|
| J-Band | Pa$\beta$ | 6.19 | 1282.20 | $\cdots$ | 187 |
| H-Band | Br10 | | em | | |
| | Br11 | 4.59 | 367.65 | $\cdots$ | |
| | Br12 | 4.22 | 352.06 | $\cdots$ | |
| | Br13 | 3.40 | 320.73 | $\cdots$ | |
| | Br14 | 2.76 | 276.09 | $\cdots$ | |
| K-Band | Br$\gamma$ | 8.18 | 285.61 | 295 | 181 |

**Table B.7.** 120 Tau - EW, Fl, and FWHM of the hydrogen lines.

| Band | Line | EW | Fl | FWHM |
|---|---|---|---|---|
| J-Band | Pa$\beta$ | 20.46 | 1019.65 | 308 |
| H-Band | Br9 | 25.75 | 359.46 | 448 |
| | Br10 | 16.84 | 302.77 | 447 |
| | Br11 | 14.64 | 300.85 | 415 |
| | Br12 | 14.14 | 311.4 | 436 |
| | Br13 | 13.19 | 304.5 | 453 |
| | Br14 | 13.20 | 324.34 | 468 |
| | Br15 | 13.41 | 345.52 | 475 |
| | Br16 | 11.01 | 286.59 | 454 |
| | Br17 | 10.07 | 267.08 | 456 |
| | Br18 | 9.09 | 243.23 | 458 |
| | Br19 | 8.45 | 230.96 | 475 |
| | Br20 | 7.27 | 201.9 | 431 |
| | Br21 | 5.75 | 162.68 | 411 |
| | Br22 | 4.18 | 121 | 384 |
| | Br23 | 3.08 | 91.63 | 329 |
| | Br24 | 1.46 | 44.76 | 331 |
| | Br25 | 0.72 | 22.39 | 246 |
| | Br26 | 0.46 | 14.59 | 228 |
| K-Band | Pf17 | | em | |
| | Pf18 | 23.96 | 121.38 | 364 |
| | Pf19 | 12.54 | 70.45 | 309 |
| | Pf20 | 13.97 | 80.41 | 465 |
| | Pf21 | 11.72 | 69.69 | 470 |
| | Pf22 | 11.74 | 72.31 | 482 |
| | Pf23 | 9.07 | 58.12 | 502 |
| | Pf24 | 6.43 | 43.04 | 421 |
| | Pf25 | 4.98 | 34.12 | 352 |
| | Pf26 | 5.08 | 35.74 | 510 |
| | Pf27 | 1.25 | 9.25 | 253 |
| | Pf28 | 1.22 | 9.05 | 224 |
| | Pf29 | 1.05 | 7.85 | 264 |
| | Br$\gamma$ | 20.55 | 220.39 | 376 |
| | Br$\delta$ | 29.53 | 405.48 | 487 |
| | Pa$\alpha$ | 81.98 | 1072.18 | 338 |
| L-Band | Hu13 | | em | |
| | Br$\alpha$ | 69.47 | 50.08 | 263 |
| | Hu14 | 35.66 | 27.62 | 435 |
| | Hu15 | 35.76 | 30.49 | 476 |
| | Hu16 | 35.41 | 33.47 | 479 |
| | Hu17 | 29.53 | 30.06 | 485 |
| | Pf$\gamma$ | 36.06 | 37.01 | 355 |
| | Hu18 | 29.28 | 30.83 | 521 |
| | Hu19 | 21.83 | 24.48 | 477 |
| | Hu20 | 19.26 | 22.12 | 482 |
| | Hu21 | 17.39 | 20.49 | 489 |
| | Hu22 | 15.05 | 18.31 | 487 |
| | Hu23 | 12.38 | 15.63 | 480 |
| | Hu24 | 10.81 | 13.96 | 529 |
| | Hu25 | 7.55 | 9.91 | 427 |
| | Hu26 | 5.72 | 7.64 | 401 |
| | Hu27 | 3.45 | 4.68 | 368 |
| | Hu28 | 2.20 | 3.02 | 216 |
| | Hu29 | 2.50 | 3.49 | 331 |
| | Pf$\delta$ | 25.92 | 41.68 | 382 |

**Table B.8.** BK Cam - EW, Fl, and FWHM of the hydrogen lines.

| Band | Line | EW | Fl | FWHM |
|---|---|---|---|---|
| J-Band | Paβ | 15.04 | 552.22 | 325 |
| H-Band | Br9 | 25.4 | 269.77 | 586 |
| | Br10 | 17.82 | 217.73 | 689 |
| | Br11 | 12.78 | 172.52 | 473 |
| | Br12 | 11.38 | 166.64 | 454 |
| | Br13 | 10.36 | 158.14 | 474 |
| | Br14 | 10.2 | 165.02 | 514 |
| | Br15 | 12.41 | 210.03 | 564 |
| | Br16 | 9.07 | 155.4 | 632 |
| | Br17 | 7.86 | 141.84 | 539 |
| | Br18 | 7.02 | 128.89 | 575 |
| | Br19 | 5.65 | 106.08 | 542 |
| | Br20 | 4.17 | 80.68 | 539 |
| | Br21 | 3.03 | 59.79 | 491 |
| | Br22 | 2.05 | 41.35 | 449 |
| | Br23 | 1.18 | 24.46 | 456 |
| | Br24-25 | | em | |
| K-Band | Pf17 | 17.39 | 68.83 | 592 |
| | Pf18 | 15.65 | 63.82 | 517 |
| | Pf19 | 12.54 | 52.83 | 545 |
| | Pf20 | 12.77 | 54.57 | 613 |
| | Pf21 | 9.76 | 42.9 | 606 |
| | Pf22 | 7.46 | 33.66 | 507 |
| | Pf23 | 5.28 | 24.41 | 518 |
| | Pf24 | 3.93 | 18.52 | 397 |
| | Pf25 | 2.99 | 14.32 | 452 |
| | Pf26 | 2.97 | 14.48 | 571 |
| | Pf27 | 1.1 | 5.44 | 299 |
| | Pf28 | 0.49 | 2.48 | ⋯ |
| | Pf29 | 0.71 | 3.59 | ⋯ |
| | Brγ | 17.88 | 119.76 | 401 |
| | Brδ | 24.03 | 221.82 | 502 |
| | Paα | 69.13 | 689.22 | 409 |
| L-Band | Brα | 50.2 | 40.22 | 303 |
| | Hu14 | 35.93 | 29.8 | 489 |
| | Hu15 | 34.39 | 31 | 553 |
| | Hu16 | 31.22 | 30.33 | 553 |
| | Hu17 | 26.45 | 27.67 | 525 |
| | Pfγ | 33.67 | 35.39 | 405 |
| | Hu18 | 22.48 | 24.24 | 527 |
| | Hu19 | 18.17 | 20.42 | 530 |
| | Hu20 | 15.62 | 17.98 | 554 |
| | Hu21 | 14.71 | 17.32 | 584 |
| | Hu22 | 10.96 | 13.35 | 558 |
| | Hu23 | 8.66 | 10.84 | 510 |
| | Hu24 | 8.39 | 10.69 | 561 |
| | Hu25 | 5.95 | 7.72 | 500 |
| | Hu26 | 4.33 | 5.69 | 514 |
| | Hu27 | 3.38 | 4.51 | 517 |
| | Pfδ | 28.09 | 45.81 | 343 |

**Table B.9.** V1150 Tau - EW, Fl, and FWHM of the hydrogen lines.

| Band | Line | EW | Fl | FWHM |
|---|---|---|---|---|
| H-Band | Br9 | 25.45 | 23.66 | 489 |
| | Br10 | 17.94 | 19.06 | 497 |
| | Br11 | 17.45 | 20.53 | 522 |
| | Br12 | 15.88 | 20.32 | 521 |
| | Br13 | 13.56 | 18.18 | 504 |
| | Br14 | 14.08 | 19.66 | 557 |
| | Br15 | 10.78 | 15.31 | 519 |
| | Br16 | 10.61 | 15.71 | 558 |
| | Br17 | 9.7 | 14.57 | 575 |
| | Br18 | 8.69 | 13.48 | 570 |
| | Br19 | 7.01 | 11.07 | 558 |
| | Br20 | 5.32 | 8.64 | 528 |
| | Br21 | 3.61 | 6.02 | 473 |
| | Br22 | 2.22 | 3.8 | 437 |
| | Br23 | 1.53 | 2.68 | 424 |
| | Br24 | 0.84 | 1.5 | 418 |
| | Br25 | 0.49 | 0.89 | 482 |
| K-Band | Pf17 | 24.38 | 9.53 | 695 |
| | Pf18 | 17.23 | 7.07 | 535 |
| | Pf19 | 15.05 | 6.34 | 582 |
| | Pf20 | 11.7 | 5.08 | 537 |
| | Pf21 | 9.32 | 4.17 | 537 |
| | Pf22 | 7.67 | 3.51 | 498 |
| | Pf23 | 5.61 | 2.61 | 509 |
| | Pf24 | 3.9 | 1.85 | 432 |
| | Pf25 | 2.85 | 1.38 | 409 |
| | Pf26 | 2.19 | 1.08 | 502 |
| | Pf27 | 1.06 | 0.53 | 345 |
| | Pf28 | 0.62 | 0.31 | 301 |
| | Brγ | 23.8 | 15.72 | 389 |
| | Brδ | 29.56 | 25.97 | 498 |
| L-Band | Hu13 | 51.98 | 5.1 | 557 |
| | Brα | 78.68 | 8.32 | 304 |
| | Hu14 | 39.76 | 4.32 | 478 |
| | Hu15 | 40.75 | 4.69 | 561 |
| | Hu16 | 36.86 | 4.52 | 607 |
| | Hu17 | 35.19 | 4.65 | 659 |
| | Pfγ | 51 | 6.81 | 479 |
| | Hu18 | 28.97 | 3.97 | 661 |
| | Hu19 | 25.11 | 3.56 | 686 |
| | Hu20 | 18.01 | 2.65 | 640 |
| | Hu21 | 16.67 | 2.51 | 676 |
| | Hu22 | 10.92 | 1.68 | 574 |
| | Hu23 | 9.77 | 1.54 | 572 |
| | Hu24 | 7.06 | 1.14 | 488 |
| | Hu25 | 4.46 | 0.74 | 388 |
| | Hu26 | 3.54 | 0.6 | 395 |
| | Hu27 | 2.21 | 0.37 | 375 |
| | Hu28 | 1.26 | 0.22 | 320 |
| | Pfδ | 44.55 | 8.59 | 418 |

**Table B.10.** 12 Vul - EW, Fl, FWHM, and $\Delta V$ of the hydrogen lines.

| Band | Line | EW | Fl | FWHM | $\Delta V$ |
|------|------|-----|-----|------|-----|
| H-Band | Br9 | | em | | |
| | Br10 | 8.52 | 51.11 | 464 | 301 |
| | Br11 | 7.88 | 53.63 | 417 | 276 |
| | Br12 | 6.69 | 50.72 | 453 | 266 |
| | Br13 | 4.96 | 40.44 | 413 | 277 |
| | Br14 | 4.18 | 36.7 | 395 | 257 |
| | Br15 | 3.05 | 26.73 | 435 | 264 |
| | Br16 | 2.23 | 20.95 | 371 | 264 |
| | Br17 | 1.82 | 17.45 | 574 | 270 |
| | Br18 | 1.35 | 13.22 | 455 | 309 |
| | Br19 | 1.5 | 15.02 | 553 | $\cdots$ |
| | Br20 | 1.19 | 12.14 | 607 | $\cdots$ |
| K-Band | Pf18 | 4.05 | 6.62 | $\cdots$ | $\cdots$ |
| | Pf19 | 6.01 | 10.2 | $\cdots$ | $\cdots$ |
| | Pf20 | 6.29 | 10.9 | $\cdots$ | $\cdots$ |
| | Pf21 | 3.46 | 6.19 | $\cdots$ | $\cdots$ |
| | Pf22 | 2.86 | 5.23 | $\cdots$ | $\cdots$ |
| | Pf23 | 2.5 | 4.7 | $\cdots$ | $\cdots$ |
| | Br$\gamma$ | 11.28 | 30.78 | 429 | 267 |
| | Br$\delta$ | 13.31 | 54.4 | 373 | $\cdots$ |
| L-Band | Hu13 | 27.62 | 8.61 | 420 | 262 |
| | Br$\alpha$ | 37.2 | 11.99 | 391 | 240 |
| | Hu14 | 23.46 | 7.82 | 439 | 263 |
| | Hu15 | 17.69 | 6.51 | 436 | 278 |
| | Hu16 | 14.34 | 5.69 | 448 | 261 |
| | Hu17 | 13.3 | 5.55 | 441 | 229 |
| | Pf$\gamma$ | 31.45 | 13.1 | 450 | 264 |
| | Hu18 | 8.8 | 3.97 | 457 | 276 |
| | Hu19 | 6.67 | 3.14 | 434 | 266 |
| | Hu20 | 4.64 | 2.28 | 433 | 231 |
| | Hu21 | 4.19 | 2.12 | 451 | 244 |
| | Hu22 | 3.96 | 2.05 | 482 | 264 |
| | Hu23 | 3.37 | 1.79 | 493 | 244 |
| | Hu24 | 2.5 | 1.36 | 458 | 247 |
| | Hu25 | 1.91 | 1.06 | 457 | 224 |
| | Hu26 | 2.1 | 1.18 | 577 | 310 |
| | Pf$\delta$ | 24.36 | 16.71 | 414 | 257 |

**Table B.11.** 28 Cyg - EW, Fl, FWHM, and $\Delta V$ of the hydrogen lines.

| Band | Line | EW | Fl | FWHM | $\Delta V$ |
|------|------|-----|-----|------|-----|
| J-Band | Pa$\beta$ | 8.78 | 172.70 | 386 | $\cdots$ |
| H-Band | Br9 | 18.55 | 95.2 | 571 | $\cdots$ |
| | Br10 | 7.99 | 51.67 | 576 | 314 |
| | Br11 | 7.04 | 53.51 | 506 | 345 |
| | Br12 | 7.08 | 58.72 | 556 | 343 |
| | Br13 | 5.87 | 52.36 | 540 | 368 |
| | Br14 | 6.56 | 61.52 | 669 | 348 |
| | Br15 | 6.18 | 60.45 | 624 | 374 |
| | Br16 | 5.25 | 52.74 | 663 | 362 |
| | Br17 | 5.02 | 51.29 | 686 | 359 |
| | Br18 | 3.87 | 40.04 | 653 | 379 |
| | Br19 | 3.1 | 32.27 | 610 | 344 |
| | Br20 | 2.79 | 29.18 | 617 | $\cdots$ |
| | Br21 | 1.96 | 20.86 | 611 | $\cdots$ |
| | Br22-23 | | em | | |
| K-Band | Pf17 | | em | | |
| | Pf18 | 11.92 | 21.86 | 600 | $\cdots$ |
| | Pf19 | 9.6 | 18.77 | 666 | 350 |
| | Pf20 | 7.5 | 14.43 | 751 | 395 |
| | Pf21 | 5.25 | 10.13 | 591 | 481 |
| | Pf22 | 3.94 | 7.74 | 545 | 357 |
| | Pf23 | 2.97 | 5.99 | 534 | 303 |
| | Pf24 | 2.32 | 4.86 | 611 | $\cdots$ |
| | Br$\gamma$ | 11.79 | 39.11 | 484 | $\cdots$ |
| | Br$\delta$ | 19.94 | 87.21 | 513 | $\cdots$ |
| | Pa$\alpha$ | 52.66 | 224.28 | 493 | $\cdots$ |
| L-Band | Br$\alpha$ | 46.79 | 20.88 | 393 | $\cdots$ |
| | Hu14 | 30.82 | 14.1 | 621 | 326 |
| | Hu15 | 26.74 | 13.46 | 621 | 336 |
| | Hu16 | 25.76 | 14 | 666 | 327 |
| | Hu17 | 19.55 | 11.5 | 611 | 341 |
| | Pf$\gamma$ | 29.47 | 17.51 | 537 | 165 |
| | Hu18 | 16.45 | 10.15 | 636 | 327 |
| | Hu19 | 13.06 | 8.45 | 612 | |
| | Hu20 | 11.53 | 7.75 | 671 | |
| | Hu21 | 8.76 | 6.1 | 608 | |
| | Hu22 | 7.13 | 5.13 | 584 | |
| | Hu23 | 6.42 | 4.75 | 621 | |
| | Hu24 | 6.95 | 5.28 | 652 | |
| | Hu25 | 5.75 | 4.47 | 642 | |
| | Hu26 | 2.37 | 1.88 | 529 | |
| | Hu27 | 3.13 | 2.53 | 632 | |
| | Hu28-29 | | em | | |
| | Pf$\delta$ | 30.6 | 30.14 | 546 | 237 |

**Table B.12.** 48 Per - EW, Fl, and FWHM of the hydrogen lines.

| Band | Line | EW | Fl | FWHM |
|---|---|---|---|---|
| H-Band | Br9 | 19.28 | 571.26 | 242 |
| | Br10 | 11.76 | 369.51 | 188 |
| | Br11 | 10.92 | 364.62 | 206 |
| | Br12 | 9.92 | 349.66 | 216 |
| | Br13 | 9.31 | 344.56 | 250 |
| | Br14 | 8.25 | 339.4 | 246 |
| | Br15 | 6.38 | 271.02 | 224 |
| | Br16 | 6.23 | 278.35 | 248 |
| | Br17 | 5.70 | 261.76 | 279 |
| | Br18 | 4.01 | 188.7 | 220 |
| | Br19 | 4.51 | 215.7 | 306 |
| | Br20 | 4.13 | 200.08 | 310 |
| | Br21 | 3.32 | 163.87 | 300 |
| | Br22 | 2.50 | 125.7 | 288 |
| | Br23 | 3.06 | 159.1 | 331 |
| | Br24-27 | | em | |
| K-Band | Pf16 | | em | |
| | Pf17 | 12.91 | 121.67 | 265 |
| | Pf18 | 12.16 | 119.86 | 288 |
| | Pf19 | 11.29 | 112.26 | 310 |
| | Pf20 | 9.38 | 95.37 | 328 |
| | Pf21 | 7.35 | 75.98 | 317 |
| | Pf22 | 6.94 | 72.56 | 359 |
| | Pf23 | 5.43 | 57.81 | 311 |
| | Pf24 | 3.64 | 39.94 | 285 |
| | Pf25 | 3.71 | 40.8 | 312 |
| | Pf26 | 3.19 | 35.11 | 341 |
| | Pf27 | 2.14 | 24.12 | 254 |
| | Pf28 | 1.48 | 16.95 | 216 |
| | Pf29 | 1.06 | 12.34 | 209 |
| | Pf30 | 1.12 | 13.14 | 306 |
| | Pf31 | 0.52 | 6.24 | $\cdots$ |
| | Pf32 | 0.53 | 6.38 | $\cdots$ |
| | Pf33 | 0.28 | 3.35 | $\cdots$ |
| | Pf34 | 0.27 | 3.21 | $\cdots$ |
| | Pf35 | 0.13 | 1.52 | $\cdots$ |
| | Br$\gamma$ | 19.73 | 287.95 | 197 |
| | Br$\delta$ | 23.39 | 504.61 | 285 |
| L-Band | Hu13 | 39.43 | 78.99 | 286 |
| | Br$\alpha$ | 107.97 | 227.92 | 170 |
| | Hu14 | 34.86 | 72.82 | 292 |
| | Hu15 | 31.41 | 71.15 | 304 |
| | Hu16 | 29.05 | 69.09 | 337 |
| | Hu17 | 24.36 | 63.10 | 337 |
| | Pf$\gamma$ | 39.96 | 104.71 | 228 |
| | Hu18 | 20.43 | 54.11 | 332 |
| | Hu19 | 18.95 | 51.69 | 358 |
| | Hu20 | 15.06 | 42.40 | 351 |
| | Hu21 | 13.58 | 39.16 | 377 |
| | Hu22 | 13.04 | 38.72 | 439 |
| | Hu23 | 8.79 | 26.83 | 347 |
| | Hu24 | 7.96 | 24.57 | 378 |
| | Hu25 | 5.07 | 15.99 | 334 |
| | Hu26 | 5.60 | 17.91 | 317 |
| | Hu27 | 3.78 | 12.22 | 326 |
| | Hu28 | 3.47 | 11.34 | 347 |
| | Hu29 | 3.86 | 12.82 | 311 |
| | Hu30 | 3.64 | 12.17 | 337 |
| | Hu31 | 3.97 | 13.49 | 449 |
| | Pf$\delta$ | 43.62 | 173.86 | 255 |

**Table B.13.** $\omega$ Ori - EW, Fl, and FWHM of the hydrogen lines.

| Band | Line | EW | Fl | FWHM |
|---|---|---|---|---|
| J-Band | Pa$\beta$ | 15.75 | 554.74 | 302 |
| H-Band | Br$_9$ | 19.28 | 210.59 | 389 |
| | Br10 | 8.96 | 112.86 | 255 |
| | Br11 | 8.44 | 114.40 | 314 |
| | Br12 | 7.17 | 104.80 | 209 |
| | Br13 | 6.21 | 95.13 | 362 |
| | Br14 | 4.62 | 78.96 | 289 |
| | Br15-20 | | em | |
| K-Band | Pf18 | 4.18 | 15.4 | 279 |
| | Pf19 | 2.42 | 9.26 | 257 |
| | Pf20 | 2.49 | 9.69 | 495 |
| | Pf21 | 1.14 | 4.51 | 342 |
| | Pf22 | 1.24 | 5.01 | 415 |
| | Pf23 | 0.99 | 4.03 | 289 |
| | Br$\gamma$ | 16.95 | 94.73 | 312 |
| | Br$\delta$ | 20.77 | 178.38 | 356 |
| L-Band | Hu13 | | em | |
| | Br$\alpha$ | 97.18 | 39.33 | 304 |
| | Hu14 | 15.92 | 7.06 | 334 |
| | Hu15 | 14.78 | 7.34 | 447 |
| | Hu16 | 12.99 | 7.33 | 458 |
| | Hu17 | 7.54 | 4.65 | 351 |
| | Pf$\gamma$ | 36.96 | 22.78 | 342 |
| | Hu18 | 4.83 | 3.23 | 314 |
| | Hu19 | 4.10 | 2.86 | 336 |
| | Hu20 | 3.81 | 2.72 | 455 |
| | Hu21 | 2.73 | 2.02 | 376 |
| | Hu22 | 2.48 | 1.9 | 414 |
| | Hu23 | 1.85 | 1.48 | 316 |
| | Hu24 | 1.31 | 1.08 | 457 |
| | Hu25 | 1.61 | 1.32 | 313 |
| | Hu26-27 | | em | |
| | Pf$\delta$ | 19.90 | 20.33 | 327 |

**Table B.14.** 48 Lib - EW, Fl, FWHM, and $\Delta V$ of the hydrogen lines.

| Band | Line | EW | Fl | FWHM | $\Delta V$ |
|---|---|---|---|---|---|
| J-Band | Pa$\beta$ | 16.46 | 599.27 | 373 | 233 |
| H-Band | Br9 | 18.72 | 229.36 | $\cdots$ | 378 |
| | Br10 | 7.16 | 102.19 | $\cdots$ | 400 |
| | Br11 | 8.22 | 126.03 | $\cdots$ | 356 |
| | Br12 | 5.70 | 92.23 | $\cdots$ | 434 |
| | Br13 | 4.69 | 80.35 | $\cdots$ | 423 |
| | Br14 | 3.91 | 73.99 | $\cdots$ | 488 |
| | Br15 | 3.84 | 77.32 | $\cdots$ | 478 |
| | Br16 | 2.98 | 61.05 | $\cdots$ | 519 |
| | Br17 | 1.74 | 37.03 | $\cdots$ | 498 |
| | Br18 | 1.49 | 32.35 | $\cdots$ | 519 |
| | Br19 | 1.12 | 25.01 | $\cdots$ | 508 |
| | Br20 | 0.93 | 21.18 | $\cdots$ | 540 |
| K-Band | Pf18 | 11.41 | 46.61 | $\cdots$ | 320 |
| | Pf19 | 9.82 | 42.6 | $\cdots$ | 262 |
| | Pf20 | 9.18 | 40.54 | $\cdots$ | 491 |
| | Pf21 | 4.62 | 21.8 | $\cdots$ | 426 |
| | Pf22 | 3.78 | 18.4 | $\cdots$ | 407 |
| | Pf23 | 3.52 | 17.18 | $\cdots$ | 484 |
| | Pf24 | 2.45 | 12.3 | $\cdots$ | 441 |
| | Pf25 | 1.26 | 6.44 | $\cdots$ | $\cdots$ |
| | Br$\gamma$ | 15.39 | 104.56 | 377 | 234 |
| | Br$\delta$ | 18.63 | 194.6 | 520 | 329 |
| | Pa$\alpha$ | 108.90 | 1201.24 | 374 | $\cdots$ |

**Table B.15.** V696 Mon - EW, Fl, and FWHM of the hydrogen lines.

| Band | Line | EW | Fl | FWHM |
|---|---|---|---|---|
| J-Band | Pa$\beta$ | 16.83 | 721.09 | 321 |
| H-Band | Br9 | 23.79 | 312.17 | 531 |
| | Br10 | 13.51 | 214.48 | 542 |
| | Br11 | 11.49 | 198.55 | 389 |
| | Br12 | 11.18 | 206 | 424 |
| | Br13 | 9.55 | 186.56 | 403 |
| | Br14 | 10.89 | 229.88 | 465 |
| | Br15 | 11.30 | 244.67 | 534 |
| | Br16 | 7.47 | 167.11 | 442 |
| | Br17 | 6.62 | 151.32 | 428 |
| | Br18 | 5.78 | 133.76 | 417 |
| | Br19 | 5.33 | 127.57 | 435 |
| | Br20 | 5.21 | 125.52 | 421 |
| | Br21 | 4.83 | 116.74 | 431 |
| | Br22 | 3.06 | 76.99 | 363 |
| K-Band | Pf17 | | em | |
| | Pf18 | 17.93 | 93.21 | 336 |
| | Pf19 | 9.78 | 53.47 | 285 |
| | Pf20 | 14.49 | 77.67 | 506 |
| | Pf21 | 10.68 | 60.41 | 472 |
| | Pf22 | 8.57 | 51.28 | 417 |
| | Pf23 | 7.39 | 45.14 | 457 |
| | Pf24 | 6.16 | 38.72 | 408 |
| | Pf25 | 5.51 | 34.58 | 351 |
| | Pf26 | 5.09 | 32.88 | 471 |
| | Pf27 | 1.90 | 12.82 | 228 |
| | Pf28 | 1.88 | 12.75 | 241 |
| | Pf29 | 1.42 | 9.65 | 232 |
| | Br$\gamma$ | 15.49 | 140.01 | 353 |
| | Br$\delta$ | 27.33 | 321.11 | 542 |
| | Pa$\alpha$ | 66.46 | 878.84 | 373 |
| L-Band | Hu13 | 28.73 | 30.68 | 409 |
| | Br$\alpha$ | 43.39 | 50.46 | 308 |
| | Hu14 | 24.58 | 30.33 | 402 |
| | Hu15 | 25.17 | 32.36 | 436 |
| | Hu16 | 25.42 | 34 | 475 |
| | Hu17 | 21.45 | 30.46 | 436 |
| | Pf$\gamma$ | 24.66 | 35.05 | 350 |
| | Hu18 | 20.52 | 30.59 | 512 |
| | Hu19 | 16.81 | 25.94 | 462 |
| | Hu20 | 14.38 | 22.54 | 432 |
| | Hu21 | 12.66 | 20.34 | 432 |
| | Hu22 | 12.67 | 20.77 | 460 |
| | Hu23 | 9.96 | 16.88 | 422 |
| | Hu24 | 10.18 | 17.6 | 468 |
| | Hu25 | 8.15 | 14.28 | 426 |
| | Hu26 | 6.59 | 11.78 | 381 |
| | Hu27 | 4.36 | 7.86 | 436 |
| | Hu28 | 3.20 | 5.83 | 388 |
| | Hu29 | 3.13 | 5.85 | $\cdots$ |
| | Hu30 | 5.27 | 9.84 | $\cdots$ |
| | Pf$\delta$ | 11.85 | 22.16 | 550 |

**Table B.16.** EW Lac - EW, Fl, FWHM, and $\Delta V$ of the hydrogen lines.

| Band | Line | EW | Fl | FWHM | $\Delta V$ |
|------|------|-----|-----|------|------|
| J-Band | Pa$\beta$ | 2.49 | 43.31 | $\cdots$ | 570 |
| H-Band | Br10 | 2.56 | 16.08 | $\cdots$ | $\cdots$ |
| | Br11 | 2.58 | 17.63 | $\cdots$ | $\cdots$ |
| | Br12 | 1.71 | 12.65 | $\cdots$ | $\cdots$ |
| | Br13 | 0.28 | 2.15 | $\cdots$ | $\cdots$ |
| | Br14-19 | | shell | | |
| K-Band | Pf17-22 | | shell | | |
| | Br$\gamma$ | 6.18 | 16.91 | 796 | 571 |
| | Br$\delta$ | 14.03 | 56.78 | 793 | 494 |
| | Pa$\alpha$ | 31.26 | 137.42 | 481 | 292 |
| L-Band | Br$\alpha$ | 63.13 | 15.52 | 328 | $\cdots$ |
| | Hu14 | 16.55 | 4.17 | 805 | 491 |
| | Hu15 | 14.08 | 4.05 | 700 | 505 |
| | Hu16 | 9.19 | 2.94 | 785 | 524 |
| | Hu17 | 9.47 | 3.22 | 471 | 496 |
| | Pf$\gamma$ | 20.65 | 7.16 | 779 | 346 |
| | Hu18 | 5.54 | 2.1 | 592 | 474 |
| | Hu19 | 6.25 | 2.55 | 656 | 479 |
| | Hu20 | 4.57 | 2 | 652 | 458 |
| | Hu21 | 3.64 | 1.7 | $\cdots$ | 552 |
| | Hu22 | 5.06 | 2.45 | $\cdots$ | 628 |
| | Hu23 | 2.66 | 1.34 | $\cdots$ | 514 |
| | Hu24 | 1.2 | 0.63 | $\cdots$ | 462 |
| | Pf$\delta$ | 17.14 | 11.65 | 717 | 420 |

**Table B.17.** *o* Aqr - EW, Fl, FWHM, and $\Delta V$ of the hydrogen lines.

| Band | Line | EW | Fl | FWHM | $\Delta V$ |
|------|------|-----|-----|------|------|
| J-Band | Pa$\beta$ | 19.77 | 603.00 | 299 | $\cdots$ |
| H-Band | Br9 | 17.52 | 174.2 | 431 | $\cdots$ |
| | Br10 | 9.44 | 102.77 | 437 | 247 |
| | Br11 | 8.26 | 102.29 | 450 | 295 |
| | Br12 | 7.33 | 99.06 | 407 | 303 |
| | Br13 | 6.84 | 98.5 | 514 | 323 |
| | Br14 | 5.73 | 91.13 | 601 | 351 |
| | Br15 | 5.50 | 90.52 | 517 | 352 |
| | Br16 | 4.04 | 67.89 | 713 | 394 |
| | Br17 | 4.13 | 71.76 | 818 | 429 |
| | Br18 | 3.38 | 59.62 | 780 | 429 |
| | Br19 | 2.28 | 40.72 | 602 | 364 |
| | Br20 | 2.66 | 47.72 | 773 | 443 |
| K-Band | Pf17 | | em | | |
| | Pf18 | 13.62 | 44.43 | 595 | 337 |
| | Pf19 | 6.23 | 22 | 564 | 349 |
| | Pf20 | 6.38 | 22.72 | 644 | 438 |
| | Pf21 | 5.24 | 18.97 | 630 | 365 |
| | Pf22 | 4.04 | 14.92 | 621 | 341 |
| | Pf23 | 3.52 | 13.11 | 708 | 327 |
| | Pf24 | 2.59 | 9.78 | 563 | 458 |
| | Br$\gamma$ | 19.43 | 100.61 | 322 | $\cdots$ |
| | Br$\delta$ | 21.22 | 166.60 | 404 | $\cdots$ |
| | Pa$\alpha$ | 112.46 | 1042.52 | 393 | $\cdots$ |

**Table B.18.** V923 Aql - EW, Fl, FWHM, and $\Delta V$ of the hydrogen lines.

| Band | Line | EW | Fl | FWHM | $\Delta V$ |
|------|------|-----|-----|------|------|
| J-Band | Pa$\beta$ | 9.21 | 17.63 | 207 | 362 |
| H-Band | Br9 | 8.7 | 5.75 | $\cdots$ | 434 |
| | Br10-14 | | em | | |
| K-Band | Br$\gamma$ | 9.98 | 3.42 | 275 | $\cdots$ |
| | Br$\delta$ | 11.93 | 6.07 | 389 | 403 |
| | Pa$\alpha$ | 60.95 | 32.55 | 333 | $\cdots$ |
| L-Band | Br$\alpha$ | 68.12 | 0.97 | 268 | $\cdots$ |
| | Hu14 | 13.41 | 0.2 | 372 | 338 |
| | Hu15 | 11.95 | 0.22 | 409 | 354 |
| | Hu16 | 9.96 | 0.22 | 484 | 370 |
| | Hu17 | 8.88 | 0.23 | 401 | 387 |
| | Pf$\gamma$ | 21.87 | 0.56 | 256 | 244 |
| | Hu18 | 6.85 | 0.2 | 420 | 339 |
| | Hu19 | 5.3 | 0.17 | 501 | 403 |
| | Hu20 | 3.83 | 0.13 | $\cdots$ | 398 |
| | Hu21 | 2.59 | 0.1 | $\cdots$ | 450 |
| | Hu22 | 4.08 | 0.16 | $\cdots$ | 381 |
| | Hu23 | 2.25 | 0.1 | $\cdots$ | 373 |
| | Hu24 | 1.84 | 0.09 | $\cdots$ | $\cdots$ |
| | Hu25 | 1.84 | 0.09 | $\cdots$ | $\cdots$ |
| | Hu26 | 0.85 | 0.04 | $\cdots$ | $\cdots$ |
| | Pf$\delta$ | 21.07 | 1.4 | 335 | 314 |

**Table B.19.** 28 Tau - EW, Fl, FWHM, and $\Delta V$ of the hydrogen lines.

| Band | Line | EW | Fl | FWHM | $\Delta V$ |
|------|------|-----|-----|------|------|
| J-Band | Pa$\beta$ | 16.16 | 368.68 | 383 | $\cdots$ |
| H-Band | Br9 | 14.73 | 102.04 | $\cdots$ | $\cdots$ |
| | Br10 | 9.43 | 76.86 | $\cdots$ | $\cdots$ |
| | Br11 | 6.73 | 61.09 | $\cdots$ | $\cdots$ |
| | Br12 | 6.34 | 61.66 | $\cdots$ | $\cdots$ |
| | Br13-23 | | shell | | |
| K-Band | Pf17 | 6.13 | 14.15 | $\cdots$ | 366 |
| | Pf18 | 3.57 | 8.45 | $\cdots$ | 448 |
| | Pf19 | 3.02 | 7.29 | $\cdots$ | 412 |
| | Pf20 | 2.4 | 5.97 | $\cdots$ | 544 |
| | Pf21 | 3.29 | 8.33 | $\cdots$ | 571 |
| | Br$\gamma$ | 16.26 | 59.77 | 387 | $\cdots$ |
| | Br$\delta$ | 17.08 | 96.17 | 401 | $\cdots$ |
| | Pa$\alpha$ | 95.23 | 623.99 | 478 | $\cdots$ |
| L-Band | Br$\alpha$ | 99.94 | 5.1 | 348 | $\cdots$ |
| | Hu14 | 17.03 | 0.88 | 619 | 363 |
| | Hu15 | 13.79 | 0.78 | 601 | 331 |
| | Hu16 | 12.7 | 0.75 | 685 | 357 |
| | Hu17 | 9.2 | 0.58 | 535 | 327 |
| | Pf$\gamma$ | 28.41 | 1.83 | 395 | $\cdots$ |
| | Hu18 | 8.49 | 0.57 | 714 | 440 |
| | Hu19 | 5.98 | 0.42 | 723 | 450 |
| | Hu20 | 5.33 | 0.38 | 733 | 420 |
| | Hu21 | 4.69 | 0.34 | 669 | 393 |
| | Hu22 | 4.54 | 0.34 | 653 | 428 |
| | Hu23 | 2.13 | 0.16 | 716 | 414 |
| | Hu24 | 2.7 | 0.21 | 675 | 363 |
| | Hu25 | 2.4 | 0.19 | 718 | 401 |
| | Hu26 | 2.38 | 0.19 | 478 | $\cdots$ |
| | Hu27 | 1.27 | 0.1 | 493 | $\cdots$ |
| | Pf$\delta$ | 26.9 | 2.69 | 691 | 408 |

## Appendix C: Metallic line parameters

**Table C.1.** Metallic line parameters.

| Element | Line [$\mu$m] | V1075 Sco | $\Psi_{01}$ Ori | $\pi$ Aqr | MX Pup | 228 Eri | 105 Tau | 66 Oph | V4024 Sgr |
|---|---|---|---|---|---|---|---|---|---|
| O I | 1.1290 | na | na | na | na | 4.41 | na | ⋯ | na |
| C I | 1.1756 | em | 1.33 | 2.31 | 0.69 | 1.23 | 2.12 | ⋯ | 0.6 |
| Mg I | 1.1828 | ⋯ | 0.53 | ⋯ | ⋯ | em | em | em? | ⋯ |
| C I | 1.1899 | ⋯ | ⋯ | ⋯ | ⋯ | 0.27 | em? | -1 | em? |
| He I | 1.1972 | -0.42 | -0.5 | ⋯ | ⋯ | -0.54 | -0.47 | -1.12 | -0.51 |
| O I | 1.2467 | ⋯ | 1.07 | 1.33 | 0.62 | 0.6 | 0.89 | ⋯ | ⋯ |
| C I | 1.2565 | ⋯ | ⋯ | 0.16 | ⋯ | 0.38 | 0.67 | ⋯ | ⋯ |
| C I | 1.2617 | ⋯ | ⋯ | em | ⋯ | 0.23 | em | ⋯ | ⋯ |
| Na I? | 1.2679 | ⋯ | ⋯ | ⋯ | ⋯ | 0.22 | ⋯ | ⋯ | 0.25 |
| He I | 1.2788 | -0.3 | -0.21 | ⋯ | -0.15 | -0.33 | -0.31 | abs | -0.98 |
| He I | 1.2972 | ⋯ | abs | ⋯ | abs | -0.28 | -0.54 | abs | -0.27 |
| O I | 1.3168 | ⋯ | 2.56 | 0.87 | 1.93 | 2.19 | 2.1 | ⋯ | ⋯ |
| Fe I | 1.5299 | ⋯ | ⋯ | ⋯ | ⋯ | ⋯ | 0.32 | ⋯ | ⋯ |
| N I | 1.5586 | ⋯ | ⋯ | ⋯ | ⋯ | ⋯ | em | ⋯ | ⋯ |
| Fe I | 1.5626 | ⋯ | 0.16 | 0.74 | ⋯ | ⋯ | 0.27 | ⋯ | ⋯ |
| Fe I | 1.5761 | ⋯ | em | 0.35 | 0.45 | ⋯ | 0.32 | ⋯ | ⋯ |
| Si I | 1.5964 | ⋯ | ⋯ | ⋯ | ⋯ | ⋯ | ⋯ | ⋯ | ⋯ |
| C I | 1.6009* | ⋯ | em | ⋯ | ⋯ | 1.25 | 1.68 | ⋯ | ⋯ |
| Si I | 1.6064 | ⋯ | ⋯ | ⋯ | ⋯ | ⋯ | ⋯ | ⋯ | ⋯ |
| Mg II | 1.6765 | ⋯ | em | ⋯ | ⋯ | em | 0.51 | ⋯ | ⋯ |
| Fe II | 1.6787 | ⋯ | em | ⋯ | ⋯ | em | 1.53 | ⋯ | ⋯ |
| Fe II | 1.6878 | ⋯ | 0.43 | ⋯ | ⋯ | 0.5 | 1.89 | ⋯ | ⋯ |
| C I | 1.6895 | ⋯ | ⋯ | ⋯ | ⋯ | 0.47 | 0.75 | ⋯ | ⋯ |
| He I | 1.7007 | ⋯ | -0.25 | ⋯ | -0.4 | -0.38 | -0.48 | ⋯ | -0.36 |
| Mg I | 1.7109 | ⋯ | 0.73 | ⋯ | ⋯ | ⋯ | 0.96 | ⋯ | ⋯ |
| O I | 1.8026 | na | em? | na | na | 2.51 | em? | ⋯ | na |
| O I | 1.8247 | na | 5.44 | na | na | 1.37 | ⋯ | ⋯ | na |
| He I | 2.0587 | 3.09 | 3.53 | shell | 2.6 | 3.64 | em | 1.9 | 2.27 |
| Fe II | 2.0892 | ⋯ | ⋯ | ⋯ | ⋯ | ⋯ | 0.53 | ⋯ | ⋯ |
| He I | 2.1126 | ⋯ | ⋯ | ⋯ | ⋯ | -0.38 | ⋯ | ⋯ | -0.75 |
| Mg II | 2.1375 | ⋯ | 1 | 0.94 | 0.8 | 0.81 | 0.68 | ⋯ | ⋯ |
| Mg II | 2.1438 | ⋯ | 1.09 | 1.05 | 0.58 | 0.7 | 1.04 | ⋯ | ⋯ |
| He I | 2.1614 | 2.39 | ⋯ | ⋯ | em? | ⋯ | ⋯ | ⋯ | ⋯ |
| Na I | 2.2062 | ⋯ | ⋯ | ⋯ | ⋯ | ⋯ | ⋯ | ⋯ | ⋯ |
| Na I | 2.2090 | ⋯ | ⋯ | ⋯ | ⋯ | ⋯ | ⋯ | ⋯ | ⋯ |
| Mg II | 2.4038 | ⋯ | em | ⋯ | na | ⋯ | em | ⋯ | ⋯ |
| Mg II | 2.4131 | ⋯ | em | ⋯ | na | ⋯ | em | ⋯ | ⋯ |
| He I | 2.4730 | ⋯ | abs | ⋯ | na | abs | abs | ⋯ | ⋯ |
| O I | 3.6620 | na | 1.53 | na | na | em? | 1.42 | ⋯ | na |
| He I | 3.7037 | na | em? | na | na | em? | ⋯ | ⋯ | na |
| C I | 3.7223 | na | ⋯ | na | na | ⋯ | 1.8 | ⋯ | na |
| Fe II | 3.8662 | na | ⋯ | na | na | ⋯ | ⋯ | ⋯ | na |
| Fe II | 3.9380 | na | ⋯ | na | na | ⋯ | em? | ⋯ | na |
| C I | 3.9886 | na | ⋯ | na | na | em? | 1.32 | ⋯ | na |
| C I | 3.9994 | na | ⋯ | na | na | em? | 2.62 | ⋯ | na |
| He I | 4.0373 | na | 2.28 | na | na | 3.42 | 2.44 | ⋯ | na |

**Notes.** The EW are in Å. em: the line is in emission but difficult to fit; abs: the line is in absorption but difficult to fit; na: spectral range not available. C I 1.6009* is C I 1.6009 $\mu$m + 1.6026 $\mu$m blended.

**Table C.2.** Metallic line parameters (continuation of C.1).

| Element | Line [μm] | 120 Tau | BK Cam | V1150 Tau | 12 Vul | 28 Cyg | 48 Per | ω Ori |
|---|---|---|---|---|---|---|---|---|
| O I | 1.1290 | 4.26 | em | na | na | em | na | ⋯ |
| C I | 1.1756 | 1.83 | em | na | na | 0.82 | na | ⋯ |
| Mg I | 1.1828 | 0.34 | ⋯ | na | na | 0.49 | na | 0.49 |
| C I | 1.1899 | em? | -1 | na | na | 0.32 | na | ⋯ |
| He I | 1.1972 | -0.31 | -0.84 | na | na | -1.07 | na | -0.75 |
| O I | 1.2467 | 1.06 | 0.98 | na | na | 0.4 | na | em |
| C I | 1.2565 | ⋯ | ⋯ | na | na | ⋯ | na | ⋯ |
| C I | 1.2617 | ⋯ | ⋯ | na | na | ⋯ | na | ⋯ |
| Na I | 1.2679 | ⋯ | ⋯ | na | na | -0.18 | na | -0.16 |
| He I | 1.2788 | -0.37 | -0.72 | na | na | -0.78 | na | -0.87 |
| He I | 1.2972 | -0.49 | abs | na | na | -0.39 | na | -0.54 |
| O I | 1.3168 | 1.84 | 1.74 | na | na | 1.2 | na | 0.58 |
| Fe I | 1.5299 | 0.25 | ⋯ | em | ⋯ | em | 0.19 | 0.18 |
| N I | 1.5586 | em | 1.33 | ⋯ | ⋯ | ⋯ | ⋯ | ⋯ |
| Fe I | 1.5626 | 0.43 | 0.87 | ⋯ | ⋯ | ⋯ | ⋯ | ⋯ |
| Fe I | 1.5761 | 1.12 | 1.44 | 0.91 | ⋯ | 0.52 | 2.19 | 0.33 |
| Si I | 1.5964 | em | 0.22 | ⋯ | ⋯ | 1.19 | ⋯ | ⋯ |
| C I | 1.6009* | em | 0.56 | ⋯ | ⋯ | 0.24 | em | ⋯ |
| Si I | 1.6064 | ⋯ | 0.68 | ⋯ | ⋯ | 0.63 | ⋯ | ⋯ |
| Mg II | 1.6765 | 0.62 | em | 0.55 | ⋯ | ⋯ | ⋯ | ⋯ |
| Fe II | 1.6787 | 1.24 | em | em | ⋯ | ⋯ | ⋯ | ⋯ |
| Fe II | 1.6878 | 1.09 | ⋯ | ⋯ | ⋯ | em | 2.59 | ⋯ |
| C I | 1.6895 | 0.72 | ⋯ | ⋯ | ⋯ | em | 1.96 | ⋯ |
| He I | 1.7007 | -0.65 | abs | -0.82 | -0.49 | -0.71 | -0.43 | -0.59 |
| Mg I | 1.7109 | ⋯ | ⋯ | ⋯ | ⋯ | ⋯ | 0.53 | ⋯ |
| O I | 1.8026 | 3.04 | 1.99 | em | ⋯ | em? | 2.54 | em? |
| O I | 1.8247 | 1.49 | 0.97 | ⋯ | ⋯ | 1.98 | ⋯ | 6.46 |
| He I | 2.0587 | 3.68 | ⋯ | 1.2 | em | 3.6 | ⋯ | 5.76 |
| Fe II | 2.0892 | ⋯ | ⋯ | ⋯ | ⋯ | ⋯ | 0.38 | ⋯ |
| He I | 2.1126 | ⋯ | abs? | ⋯ | ⋯ | ⋯ | ⋯ | -0.63 |
| Mg II | 2.1375 | 1.1 | ⋯ | 0.53 | ⋯ | ⋯ | 0.55 | 0.3 |
| Mg II | 2.1438 | 0.89 | ⋯ | 0.38 | ⋯ | ⋯ | 1.2 | 0.2 |
| He I | 2.1614 | ⋯ | ⋯ | ⋯ | ⋯ | ⋯ | abs? | abs? |
| Na I | 2.2062 | ⋯ | ⋯ | ⋯ | ⋯ | ⋯ | 0.28 | ⋯ |
| Na I | 2.2090 | ⋯ | ⋯ | ⋯ | ⋯ | ⋯ | 0.37 | ⋯ |
| Mg II | 2.4038 | em | em | ⋯ | ⋯ | ⋯ | ⋯ | ⋯ |
| Mg II | 2.4131 | em | em | ⋯ | ⋯ | ⋯ | ⋯ | ⋯ |
| He I | 2.4730 | abs | ⋯ | ⋯ | ⋯ | abs | ⋯ | ⋯ |
| O I | 3.6620 | 1.45 | 0.59 | 0.52 | ⋯ | em | 0.28 | ⋯ |
| He I | 3.7037 | ⋯ | em | ⋯ | ⋯ | ⋯ | ⋯ | ⋯ |
| C I | 3.7223 | ⋯ | ⋯ | ⋯ | ⋯ | ⋯ | 3.52 | ⋯ |
| Fe II | 3.8662 | ⋯ | ⋯ | ⋯ | ⋯ | 0.52 | 4.69 | ⋯ |
| Fe II | 3.9380 | ⋯ | ⋯ | ⋯ | ⋯ | ⋯ | 1.29 | ⋯ |
| C I | 3.9886 | ⋯ | ⋯ | ⋯ | ⋯ | ⋯ | 6.09 | ⋯ |
| C I | 3.9994 | ⋯ | ⋯ | ⋯ | ⋯ | ⋯ | 7.21 | ⋯ |
| He I | 4.0373 | 1.76 | em | 1.51 | 1.07 | 1.2 | 5.97 | -1.76 |

**Table C.3.** Metallic line parameters (continuation of C.1).

| Element | Line [μm] | 48 Lib | V696 Mon | EW Lac | o Aqr | V923 Aql | 28 Tau | HD 171623 |
|---------|-----------|--------|----------|--------|-------|----------|--------|-----------|
| O I | 1.1290 | 6.08 | 5.03 | ⋯ | em | em | em | ⋯ |
| C I | 1.1756 | 1.11 | 3.83 | ⋯ | 0.71 | ⋯ | 0.79 | ⋯ |
| Mg I | 1.1828 | em | 1.94 | ⋯ | 0.5 | ⋯ | em | ⋯ |
| C I | 1.1899 | ⋯ | 1.36 | ⋯ | 0.29 | ⋯ | ⋯ | ⋯ |
| He I | 1.1972 | -0.96 | -0.82 | -0.91 | ⋯ | ⋯ | ⋯ | ⋯ |
| O I | 1.2467 | 0.75 | 1.38 | 0.14 | 0.31 | 0.33 | 0.42 | ⋯ |
| C I | 1.2565 | ⋯ | 0.86 | ⋯ | 0.31 | ⋯ | ⋯ | ⋯ |
| C I | 1.2617 | ⋯ | 0.58 | ⋯ | 0.05 | ⋯ | ⋯ | ⋯ |
| Na I | 1.2679 | ⋯ | ⋯ | 0.25 | -0.11 | em | ⋯ | -0.38 |
| He I | 1.2788 | abs | ⋯ | ⋯ | ⋯ | ⋯ | ⋯ | ⋯ |
| He I | 1.2972 | abs | ⋯ | -0.57 | ⋯ | ⋯ | ⋯ | ⋯ |
| O I | 1.3168 | 1.86 | 1.6 | 0.77 | ⋯ | 0.18 | -0.79 | ⋯ |
| Fe I | 1.5299 | ⋯ | 0.46 | ⋯ | em | ⋯ | ⋯ | ⋯ |
| N I | 1.5586 | ⋯ | ⋯ | em | ⋯ | ⋯ | 0.3 | ⋯ |
| Fe I | 1.5626 | ⋯ | em | em | ⋯ | ⋯ | ⋯ | ⋯ |
| Fe I | 1.5761 | 2.25 | 3.87 | 0.09 | 0.65 | 0.72 | 0.39 | ⋯ |
| Si I | 1.5964 | ⋯ | 1.71 | ⋯ | ⋯ | ⋯ | ⋯ | ⋯ |
| C I | 1.6009* | 1.05 | 3.4 | ⋯ | ⋯ | ⋯ | ⋯ | ⋯ |
| Si I | 1.6064 | ⋯ | ⋯ | ⋯ | ⋯ | ⋯ | ⋯ | ⋯ |
| Mg II | 1.6765 | em | 0.63 | ⋯ | ⋯ | ⋯ | ⋯ | ⋯ |
| Fe II | 1.6787 | em | em | ⋯ | ⋯ | ⋯ | ⋯ | ⋯ |
| Fe II | 1.6878 | 1.98 | 1.95 | ⋯ | 0.86 | 0.77 | 2.48 | ⋯ |
| C I | 1.6895 | 0.58 | 1.95 | ⋯ | ⋯ | ⋯ | 0.92 | ⋯ |
| He I | 1.7007 | -0.85 | abs | -1.79 | ⋯ | ⋯ | ⋯ | ⋯ |
| Mg I | 1.7109 | ⋯ | 0.53 | ⋯ | em? | em | 0.7 | ⋯ |
| O I | 1.8026 | ⋯ | 3.91 | ⋯ | em? | ⋯ | ⋯ | na |
| O I | 1.8247 | ⋯ | em? | 9.36 | em? | ⋯ | ⋯ | na |
| He I | 2.0587 | -0.96 | 2.25 | shell | 0.59 | 0.36 | ⋯ | ⋯ |
| Fe II | 2.0892 | 0.63 | 0.52 | ⋯ | em | 0.22 | ⋯ | ⋯ |
| He I | 2.1126 | -0.5 | abs? | -1.31 | ⋯ | ⋯ | ⋯ | ⋯ |
| Mg II | 2.1375 | 0.71 | 1.05 | ⋯ | ⋯ | ⋯ | ⋯ | ⋯ |
| Mg II | 2.1438 | 1.01 | 2.06 | ⋯ | ⋯ | ⋯ | ⋯ | ⋯ |
| He I | 2.1614 | ⋯ | ⋯ | ⋯ | ⋯ | ⋯ | ⋯ | ⋯ |
| Na I | 2.2062 | ⋯ | 1.78 | ⋯ | ⋯ | ⋯ | ⋯ | ⋯ |
| Na I | 2.2090 | ⋯ | 0.95 | ⋯ | ⋯ | ⋯ | ⋯ | ⋯ |
| Mg II | 2.4038 | ⋯ | ⋯ | ⋯ | ⋯ | ⋯ | ⋯ | ⋯ |
| Mg II | 2.4131 | ⋯ | ⋯ | ⋯ | ⋯ | ⋯ | ⋯ | ⋯ |
| He I | 2.4730 | abs | ⋯ | ⋯ | abs | ⋯ | ⋯ | ⋯ |
| O I | 3.6620 | na | em | 0.92 | na | em? | ⋯ | na |
| He I | 3.7037 | na | ⋯ | abs? | na | ⋯ | ⋯ | na |
| C I | 3.7223 | na | 4.24 | ⋯ | na | ⋯ | 2.85 | na |
| Fe II | 3.8662 | na | 5.92 | ⋯ | na | ⋯ | 3.72 | na |
| Fe II | 3.9380 | na | 0.8 | ⋯ | na | ⋯ | 4.15 | na |
| C I | 3.9886 | na | 3.33 | ⋯ | na | em? | 2.3 | na |
| C I | 3.9994 | na | 3.36 | ⋯ | na | em? | 3.43 | na |
| He I | 4.0373 | na | 5.97 | 1.57 | na | 1.77 | 4.83 | na |